Challenges of Engineering Applications of Descriptive Geometry

Zsuzsa Balajti *

Posted Date: 3 November 2023

doi: 10.20944/preprints202311.0201.v1

Keywords: tool wear measurement; CCD cameras positioning; digitized images; reconstruction problem; Monge mapping; projector lines; mathematical correspondence; directed angle triple; Monge cuboid; bijective subset

Article

Challenges of Engineering Applications of Descriptive Geometry

Zsuzsa Balajti

Institute of Mathematics, University of Miskolc, 3515 Miskolc, Hungary; zsuzsanna.ovarine.balajtizs@uni-miskolc.hu

Abstract: Descriptive geometry has indispensable applications in many engineering activities, some of which are presented in the first chapter of this paper in order to place the development presented here among them. As a result of the continuous variability of the technological environment according to various optimization aspects, the engineering activities must also be continuously adapted to the changes, which an appropriate approach and formulation are required from the practitioners of descriptive geometry, and can even lead to improvement in the field of descriptive geometry. The imaging procedures are always based on the methods and theorems of descriptive geometry. Resolving contradictions in spatial geometry reconstruction research is a constant challenge, to which a possible answer in many cases is the search for the right projection direction. A special method of enumerating the possible infinite viewpoints for the representation of the surface edge curves is presented in another part of the paper. The procedure for determining the correct directions in a mathematically exact way is also presented through examples. The analysis and some of the results of the Monge mapping, which is suitable for the solution of a mechanical engineering task to be solved in a specific technical environment, are also presented.

Keywords: tool wear measurement; CCD cameras positioning; digitized images; reconstruction problem; Monge mapping; projector lines; mathematical correspondence; directed angle triple; Monge cuboid; bijective subset

1. Introduction

One of the objectives of this paper is to point out the constantly renewing challenges of engineering communication, which can sometimes be accompanied by the need for a new aspect-based approach to the descriptive geometry, which forms a basis for engineering communication. Today's technological progress requires the continuous renewal of knowledge necessary for the operation and development of more modern devices, primarily engineering knowledge. The communication of engineering activities is carried out the technical drawing based on descriptive geometry independent of the device, but it is always done on the 2D plane with a mutually clear correspondence between the elements of the 3D space and the elements of the 2D plane (supplemented by additional informative data). One of the many challenges of descriptive geometry is the recognition, which Stachel [1] highlighted, that although descriptive geometry drawings are "hand-made", this is not the essence of descriptive geometry, because even Gaspar Monge, from whom descriptive geometry is derived, did not refer to manual drawing as an essential element of descriptive geometry [2]. We should not be fooled by the fact, that even with the introduction of 3D-CAD/CG, the essence of hand-drawing descriptive geometry is that one of the most useful ways to facilitate understanding and firmly fix memories is to simultaneously use the senses, namely the "eyes" and motor organs, such as the „hand", since these things are connected in a similar way when acquiring any type of knowledge [3]. In the field of brain and nervous system research, visual perception and its modeling, the control of visual perception and the learnability of visual perception has been investigated, furthermore the connection between visual perception and consciousness has been analyzed [4]. According to Stachel, "Descriptive Geometry is the interplay between the 3D situation and its 2D representation, and between intuitive grasping and rigorous logical reasoning" [1]. Therefore, in addition to the theory of projection, descriptive geometry also includes the modeling techniques of curves and surfaces, as well as the intuitive approach of elementary differential geometry and 3D analytical geometry. Descriptive geometry has two main purposes. The first is to

 doi:10.20944/preprints202311.0201.v1

provide a method of imaging 3D objects, while the second aim is to give a way to recognize body shapes from their exact description, as well as to derive truths, mathematical regularities arising from their shape and position. Orthogonal projection is the most commonly used method for mapping 3D space onto a 2D plane. In the case of orthogonal projection onto a plane the orthogonal projection of the physical "real" surfaces of Euclidean space onto a plane has been usually supplemented with elevation data. Cartography, geodesy, mining, road and railway construction, river regulation, as well as the solution of certain tasks in forestry require a special representation method of descriptive geometry, the one view representation with the indication of elevations [5]. During research conducted in the field of earth sciences, cartographic data is supplemented with a large amount of information during the recording and analysis of the results of seismic monitoring measurements [6]. The field observations of the topography supplemented with measurement data require global optimization tools and robust statistical techniques to manage the data and extract additional information in order to build an extended groundwater flow model of the research area [7]. The topographic representation of the complex surface of the terrain is the basis of digital elevation models, DEMs according to the professional terminology, in which case there is a risk of losing a large amount of detailed topographical information due to traditional interpolation methods. To avoid the loss of a large amount of detailed topographic information due to traditional interpolation methods, a new method based on sliding windows had been proposed to improve the resolution of DEMs [8]. In another research area, the microtopography of machined surfaces is measured using sensor technology, based on metric orthogonal projection. The effect of the use of a round milling insert on the surface topography was studied at different cutting speeds. The surface roughness can be determined from the trace of the tool geometry on the workpiece taking into account the kinematics depending on the different cutting speed and possibly other process characteristics. By changing the surface roughness, the friction between the motion-transmitting machine parts, the wear and corrosion resistance, and the creep strength of the parts can be influenced [9]. Although the evaluation of surface quality is applied with 2D parameters during engineering practice, the analysis of the microtopography of the curved surfaces with a 3D optical microscope also provides information about the integrity of the surface, for which it is also necessary to determine the appropriate viewpoints [10]. In an additional area of research, finite element tests of a 2D cross-section are carried out for the analysis of 3D cylindrical industrial facilities and the physical phenomena occurring in them, for example also in thermal models prepared for individual industrial applications. In a lumped heat capacity model prepared for transient heat convection analysis in cross-air flow, the Finite Element Analysis simulations used with the ANSYS Fluent code are also performed in 2D sections, the results of which also show that the geometric shape of the 2D section has a clear effect on heat loss as well [11]. Among the types of multi-view representation, the two-view Monge representation is the most frequently used during engineering activities [12]. The most important informational value of the descriptive geometric procedures is that the dimensions and location of the spatial shapes can be clearly determined (provided with additional information, such as regarding their movement) [13]. Monge realized that descriptive geometry has a great importance in the field of engineering, and the treatment of space in this way also gives rise to the study of the properties of curves. Though most of the lines in any industrially created objects are the straight lines, using of the curves is so frequently required that the designer should always be prepared to apply them with confidence and competence. Facility in handling curved lines can come only as effect of the accurate knowledge of the general principles for governing of the curves generation or from practice on some concrete cases. One of Monge's most talented students was Theodore Olivier, who is primarily known for creating three-dimensional moving models of descriptive geometric processes. Olivier's moving models led to the study of movement transmission by means of descriptive geometry, which provided the basis for differential geometric analyses [14]. The time stability of steps leading to Olivier's results can also be excellently observed in the typical case of the generation of 2D curves, according to which the interpretation of the synthetic geometric evolution of the roulettes is the basis of their analytical definition. For the computer 2D graphic representation and 2D animation of roulettes, their analytical formulation based on their synthetic geometric analysis is required, which leads all the way to the topic of related surface pairs and the gearing [15]. According to Olivier's theory, an imaginative collaboration between the physical implementation of the synthetic geometric evolution of roulettes and the virtual display of its analytical determination can be realized by

 doi:10.20944/preprints202311.0201.v1

operating drawing robots controlled by Dynamic Geometry Software developed for this purpose and operated with adjustable drive pairs [16]. The tooth profile of elliptical gears with a continuously variable gear ratio has a special geometry, because instead of the "standard" circular involute it is an ellipse involute, and the 3D printed model of which was also created to support the developed process based on its mathematical geometrical definition [17]. The changing ratio noncircular gear drives are imaginative machine parts that offer a wide range of applications. In some special engineering fields, these solutions can have many advantages over traditional solutions, which have been determined using the transported lines of actions, resulting in variable axis distance and tooth profile [18], or even by applying the basic law of gearing, the function of alternating profile offsets at the constant axis distance was determined within certain limits [19]. In the field of novel approaches to the design of space curves corresponding to the most diverse boundary conditions, such as the optimization of the movement paths of robot arms, the industry constantly floods researchers with challenges. An up-to-date hybrid algorithm has been developed in its geometrically also new approach, which determine that trajectory of the robot arm from the space of possible trajectories with the lowest cycle time between two given points, avoiding obstacles [20]. The determination of the twisting, which replaces the movement between two different positions of the motion trajectories, was also inserted into the constructive geometric model developed for the investigation of kinematic drive pairs with the descriptive geometrical methods [21]. Following Theodore Olivier's way of thinking, that theoretical mathematical research should be tuned to physical realizations, the definition and visualization of the time-like axis of helical hypersurfaces [22] is also a possible connection point between the mathematical and engineering research field. The effectiveness of the knowledge of the momentary torsion axis and the design of the descriptive geometric design is demonstrated among other things, by the use of views following the motion transmission processes when determining the drive pin profile for eliminating the thread pitch fluctuation in the case of machining the spiroid worm with axis adjustment. In case of machining with traditional thread grinding, the creator straight line of the reference cone of the conical worm must be placed onto the path of the thread grinder, namely its axis must be set with the half opening angle of the reference cone. The motion transfer that changes the direction has been produced with a drive pin. The momentary screw axes of the time-dependent relative motion of interconnected space systems allow us to infer the momentary poles in the corresponding views. In the corresponding views, the radius drawn from the momentary pole to the moving point is perpendicular to the trajectory tangent. By selecting the appropriate length of the tangent, the drive pin profile can be constructed, namely accurately calculated, in an explicit form [23]. By defining the spatial kinematics method for following the operation of the drive pairs with mathematical precision, in the mathematical model built on well-understood views, the tooth surface points of the gear wheel connected to the Archimedean worm can be generated with the numerical procedure developed for this purpose, which is a mathematical geometrical modeling of the gear tooth surface [24]. The second of the two main purposes of descriptive geometry is to improve the mathematical visual perception of objects in three-dimensional space [25]. For the modeling procedures of the imaging of spatial objects, several concepts worthy of consideration have been created [26]. A serious challenge for technical optical research is to harmonize the operation of imaging optical systems and the toolbox of geometric optics with mathematical formulas in such a way that, by following the imaging processes perceptible to the human eye, it helps visual recognition in while also supporting the evolving of geometric awareness [27]. Several computer imaging techniques already exist to simulate the critical property of human vision, that vision is imperfect due to highly effective wave front aberrations that vary from person to person. In addition to existing vision simulation techniques, there are many new challenges in rendering algorithms to simulate aberrant human vision [28]. An exact solution for connecting visualization with conscious geometric interpretation is computer-enhanced descriptive geometry (CeDG), a modern scientific approach to solving and creating computer modelling of three-dimensional (3D) geometric systems through descriptive geometry procedures. The contribution of the new approach to the field of science is the inheritance of the laws of projective geometric invariants bearing the signs of duality, which ensure reliability and accuracy at the same time. To support the theoretical foundations, the procedure has been also presented by determining the intersection curve of two surfaces in a parametric implicit functional form [29]. A special form of modelling was published during a promising research of three-dimensional virtual data visualization

 doi:10.20944/preprints202311.0201.v1

tools and methods. A number of concepts have been created for modelling spatial objects, which are widely recognized [31]. The relationships of the different file formats that can be used as input data was represented using a sphere-based visualization technique, the ends of the nodes were placed on the sphere and the relationships was displayed with tube-like surfaces [32]. During the creation of a model of an existing physical 3D object, one of the many problems that arise can be classified as difficulties related to the geometric accuracy of the data and the visualization quality of the result. The main reason mentioned for modelling problems is that current computer-aided design (CAD) softwares do not possess enough tools to accurately map the measurement data of an object to be modelled. For this reason, the process of 3D modelling consists of a relatively large proportion of manual work, such as when arranging individual points and in the case of approximation of curves and surfaces. In some cases, it is necessary to generalize the model in the CAD system, which worsens the accuracy and field data quality. As a possible solution, the use of topological codes and the use of the new special CAD services created was also proposed in a study by Bartonek and co-authors [33]. Professional use of CAD modelling programs is only possible for people skilled in descriptive geometry due to communication based on views [34]. Just as the importance of mathematical knowledge continues to increase with the transfer of calculation work to computers, an increasingly high level of geometrical knowledge is also required to operate it increasingly sophisticated modelling software [35-38]. The spatial form imagined by the mathematical geometric definition is realized during the physical implementation, namely during industrial production, influenced by many factors connected to technological and production processes [39]. One possible abstract formulation of this process is mathematical geometric modelling [40]. The mathematical geometric parameters of the surfaces of the parts are supplemented during production with a number of technological and processing parameters that can cause the surface of the manufactured part to differ from the defined ideal surface. Among other things, *production geometry* deals with the theory of the geometry of tools that machine the industrial parts, the examination and analysis of the deviation of the surfaces of physically manufactured parts from the geometrically defined surfaces of the parts, and the development of their manufacturing process, all which are based on descriptive geometry. For production geometry challenges, an acceptable answer must be given every time within the limitations of the technological environment and the possibilities given by the various resources, which always shows the smallest possible deviation between the manufactured and the mathematically defined surface of the part. Olivier's research was unique for a long time in the two main fields of the tooth-generation theory of mechanisms, in the scope of the meshing conditions of the toothed elements and their manufacturing geometry. In his work published in 1842, he even separated the tooth surface theory from the analytical (mathematical) and enveloping (geometrical) methods [41]. According to his interpretation, "the question of tooth meshing belongs completely to the descriptive geometry". According to Gohman, “the tooth theory is a special part of the mathematical discipline”, where the researcher, in contrast to other areas of mathematics science, – “should take small steps looking for the new safety fixed points at each step. The worth of both scientists in creating the foundations of today's spatial tooth theory is indisputable [40]. In the research field of the worm gear drives a "Worm Scientific School" has been established at the University of Miskolc, producing 13 defended doctoral dissertations. Synthetic geometry supported by analytical geometry was applicated to analyze the structure and operation of technical constructions, such as for the production geometry development of the elements of conical and cylindrical worm gear drive pairs during the creation of the constructive geometric model. The mathematical geometric generation of helicoidal surfaces in the constructive geometric model shows a direction for the development of the correct machining of cylindrical and conical worms and the development of their production geometry [42]. A typical example of the production geometry examinations is when the modified geometric parameters of spur gears having normal evolvent teeth and the technological parameters were compared with the manufacturing parameters to reveal the correlations in order to advance the technological design [43]. In the industry, instead of the elemental toothing created by mutual enveloping, so-called profile offset toothing is often used, which can increase the load capacity and prevent malfunctions. However, since there is no solution that is favorable from all aspects at the same time for the selection of the profile shift coefficients, the basis of the decision is always a careful consideration of the operating conditions and the expected damages. However, with appropriate objective functions, it is possible to take into account several

Preprints (www.preprints.org) | NOT PEER-REVIEWED | Posted: 3 November 2023 doi:10.20944/preprints202311.0201.v1

aspects at the same time to choose the profile shift coefficient, including the suitable lubricating film thickness, linear wear, gear tooth bending stress, and Hertzian stress, which affect tooth damage and operating conditions [44]. The production geometry of the elements of the conical worm gear drive is a serious challenge, especially in connection with the analysis of the undercutting. The boundary line of the curvature interference has been investigated for the tooth surface of the wheel enveloped by a conical helicoid surface. By analyzing the effect of the main design parameters on the curvature interference, the positions on the concave tooth surface of the gear with a chance of undercutting were delimited [45]. The detailed contact analysis between the worm gear tooth surface with the evolvent worm tooth surface can be made by applying the mathematical model for the dynamical analysis of the involute cylindrical worm gear drive tests regarding the load. With the torsional oscillating dynamical model, which clearly follows the geometric interpretation, the influence of the geometric parameters can be investigated on the calculation of deviations, velocities or accelerations at any random node of the dynamic model, and together with other dynamic characteristics the position of the lubricant in the contact zone between the tooth surfaces can be analyzed, because if it is displaced, metal contact and wear occur [46]. The geometry of the worm tooth has a significant effect on the design of the lubricating wedge, which is important in terms of increasing wear resistance, service life and efficiency [47]. The drive pair elements operating surfaces are produced by enveloping its machining tool surface. The increase in the variety of technological solutions also requires the continuous adaptation and investigating of tool geometry. And the development of tool geometry itself carries the geometrical challenges of descriptive geometry. The idea of the theoretical analysis of the descriptive geometry was related to the wear test of the tool, which was carried out by our Worm Scientific Research Group in the DifiCAD Engineering Office, which has a cooperation agreement with the University of Miskolc. A special approach to ensuring reconstruction from digitized images was proposed in the field of tool geometry research related to our Worm Scientific Research Group. Measuring the wear of the cutting edge of the tool with only one CCD (Charge-coupled Device) camera and a distance meter placed next to its lens already brought doubts about the accuracy of the measurement [48]. It is preferable in terms of geometric accuracy to test the cutting-edge wear based on the true-to-size Monge representation with images taken with two CCD cameras positioned at right angles to each other, as can be seen in Figure 1.

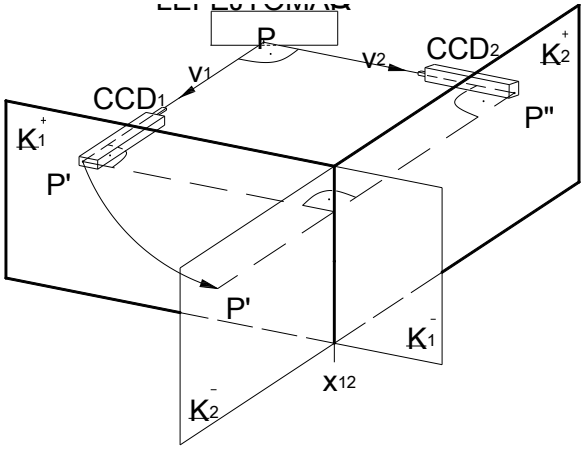

Figure 1. Schematic layout of the relationship between the images taken by CCD cameras in perpendicular direction to each other located in the direction of $\mathbf{v}_1$ and $\mathbf{v}_2$ projector lines and the Monge mapping.

For a given cutting edge curve, the image plane system can be taken up in an infinite number of ways.

Definition 1. *An image plane system $\{\underline{K}_1, \underline{K}_2\}$ consisting of mutually perpendicular image planes together with the first projector line v_1 perpendicular to the first image plane, and the second projector line v_2 perpendicular perpendicular to the second image plane defines a Monge projection.*

Hereinafter the statements are made using the term defined in this way. Therefore, not only the image plane system, but also the Monge projection can be used for a g curve in an infinite variety of

Preprints (www.preprints.org) | NOT PEER-REVIEWED | Posted: 3 November 2023 doi:10.20944/preprints202311.0201.v1

ways. The formulated task was to determine the criteria for those positions of the image plane systems of the Monge representation relative to an object fixed in the space, which criteria should be met so that the fixed object of the space can be clearly reconstructed only from the two projections on the image planes of the Monge representation without any other information.

2. Method of ensuring the bijectivity of Monge's representation by defining the directions of the views

The need to investigate bijectivity has been created by the requirement to reconstruct digitized Monge images during the research work in. Spatial objects are represented by their surface edges and lines, so as a first step the examination should be limited to these. As long as Monge's representation of the point is always clear if the generally known conventions are met, anomalies may arise in the practical application of descriptive geometry, for example during the reconstruction of curves, which must be consciously kept in mind. For example, neither the representation of a circle in general location nor the representation of a profile straight line is clear due to reconstruction complications, so the reconstruction in these cases is not clear from only two digitized images without additional information. For these and similar occurrences the descriptive geometry has found special clarifications to ensure bijectivity up to now. In the case of curve mapping, the reconstruction may require some additional information such as correspondence marking. To ensure the reconstruction during the representation of the curves, in accordance with engineering expedient thinking, the appropriate placement of the image plane system was formulated as tasks.

2.1. Examining the spatial curve

In the case of the Monge representation of the differential geometrically interpreted g curve, one coordinate plane of a Cartesian coordinate system is fitted to each image plane of the Monge representation, namely the [xy] coordinate plane onto the first image plane $\underline{K}_1$ and the [yz] coordinate plane onto the second image plane $\underline{K}_2$. Then the *y* coordinate axis is the intersection straight line of the two image planes, namely the x_{12} axis.

Theorem 1. *If the image curves g′ and g″ of the curve g can be written separately with the functions* $y \rightarrow f_1(y)$ *and* $y \rightarrow f_2(y)$ *in the corresponding Cartesian coordinate planes of the image planes, where* $x = f_1(y)$ *and* $z = f_2(y)$ *, i.e. its points have coordinates* $P\,(f_1(y), y, f_2(y))$*, then any part of the curve g can be clearly reconstructed from its images.*

A sketch of the curve, which can be clearly reconstructed from its projections, is shown in Figure 2.

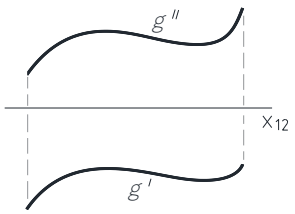

Figure 2. Bijective representation of the *g* curve.

Proof of Theorem 1. The function is such a subset of the Descartes product in which there is no identical first term and no different second terms. Therefore, to one y there is assigned only one $f_1(y) \equiv P'$ fitting to the plane $[xy] \equiv \underline{K}_1$ and one $f_2(y) \equiv P''$ fitting to the plane $[yz] \equiv \underline{K}_2$. These lines assigning P′ and P″ to one value of y are located perpendicular to the $y \equiv x_{12}$ axis. Thus, after the merging of the image planes $\underline{K}_1$ and $\underline{K}_2$, the (P′,P″) forms an ordered pair of points to which only one spatial point P belongs. Therefore, any point of the curve g and thus any part of it can be clearly reconstructed. □

Corollary 2. *If the images g′ and g″ of a curve g in the O[x, y, z] coordinate system of a Monge projection can be written separately as functions of* $y \rightarrow f_1(y)$ *and* $y \rightarrow f_2(y)$*, then no single profile plane of the Monge projection intersects more , as one point each from g′ and g″.*

Preprints (www.preprints.org) | NOT PEER-REVIEWED | Posted: 3 November 2023 doi:10.20944/preprints202311.0201.v1

Theorem 3. *If image curves g′ and g″ of the curve g cannot be written in the corresponding Cartesian coordinate planes as function $x = f_1(y)$ and $z = f_2(y)$, respectively the assignments and $y \to f_1(y)$ and $y \to f_2(y)$ are not functions, then there is a part of curve g, that cannot be clearly reconstructed from its two images.*

A sketch of the curve, which cannot be clearly reconstructed from its projections without additional information, is shown in Figure 3.

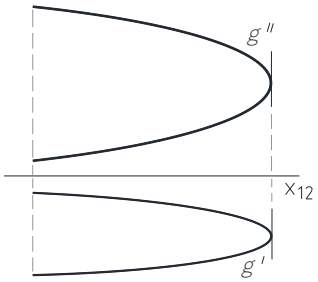

Figure 3. Non bijective representation of *g* curve.

Proof of Theorem 3. Since the projected curves *g′* and *g″* of the spatial curve *g* cannot be formed as functions, but of course they are curves, on the corresponding Cartesian coordinate planes, therefore one y has several $f_1(y) \equiv P'$ points lying on the plane $[xy] \equiv \underline{K}_1$ and several points $f_2(y) \equiv P''$ lying on the plane $[yz] \equiv \underline{K}_2$. These image points P′ and P″ fitting to a recall line perpendicular to the axis $y \equiv x_{12}$ can optionally be arranged to form ordered pairs of points, to which the spatial points P belong. So, there exists a point of the curve *g* and a neighbour of the point that cannot be reconstructed from only two images. □

Corollary 4. *If the image curves g′ and g″ in the corresponding coordinate planes of the given Cartesian coordinate system cannot be written as functions $x = f_1(y)$ and $z = f_2(y)$ then*
1. there exist profile planes of the Monge projection that intersect the curve g in more than one point, and
2. there is at least one profile plane tangent to g.

Theorem 5. *If one of the image curves g′ and g″ of the curve g cannot be written in the corresponding Cartesian coordinate plane as a function $x = f_1(y)$ or $z = f_2(y)$ but the other image is a double projection, and this can be written as functions $z = f_2(y)$ or $x = f_1(y)$, then any part of g can be clearly reconstructed from only two images.*

A sketch of the projections of such a curve can be seen in Figure 4, that one image of this curve cannot be written as a function on the corresponding Cartesian coordinate plane, but the other image is a double projection, that can be written as a function, then any part of the curve can be clearly reconstructed from only its two images.

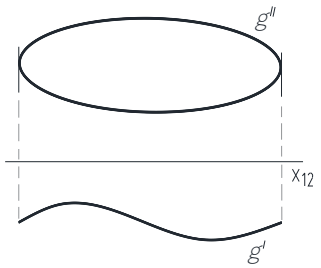

Figure 4. Representation of the *g* curve in case of double projection of one of its images.

Proof of Theorem 5. *1. Assume that g′ is a double projection among the image curves g′ and g″ of the curve g, and it can be written as a function $x = f_1(y)$, and the g″ cannot be written as a function $z = f_2(y)$ on the corresponding Cartesian coordinate plane. In this case, one y corresponds to a point $f_1(y) \equiv P'$ fitting to the plane $[xy] \equiv \underline{K}_1$ and several points $f_2(y) \equiv P''$ fitting to the plane $[yz] \equiv \underline{K}_2$. These one P′ and several P″ points located perpendicular to the $y \equiv x_{12}$ axis can be assigned to each other to form ordered pairs of points, to which several*

 doi:10.20944/preprints202311.0201.v1

spatial P points belong. Thus, any point of the curve g and thus any part of it can be clearly reconstructed from only two images.
2. If the image curve g″ is a double projection, which can be written as a function z = $f_2(y)$ and g′ cannot be written as a function x = $f_1(y)$ the proof is the indices 1 and 2, as well as ′, and ″ can be done in the same way as case 1 by exchanging the signs. □

Corollary 6. *If one of the image curves g′ and g″ of the curve g cannot be written in the corresponding Cartesian coordinate plane as a function x = $f_1(y)$ or z = $f_2(y)$, but the other image is a double projection, and this can be written as a function z = $f_2(y)$ or x = $f_1(y)$, then there is at least one profile plane that touches g.*

Theorem 7. *If the curve g does not have a tangent parallel to the profile straight directional, then the representation of any part of the curve is bijective.*

Proof of Theorem 7. *If the curve g does not have a tangent in the profile direction, this means that the tangent at any point P_0 with parameter u_0 of its images is not in the direction of the recall line, namely the recall line intersects the examined curve in point P_0. So, there is no point P_0 of the curve g with parameter u_0, in the region of which all points P_{-1} and P_1 with parameters u_{-1} and u_1 are located on one side of the recall line of the point P_0, where $u_{-1}<u_0<u_1$. This means that there is no curve segment that has two points on a recall straight line. Because each recall straight line has only one point on the curve g, any point on curve g can be reconstructed from its two images, which means that the representation of the curve is bijective.* □

All of this follows from the fact that not all points of a curve can be marked with letter and comma.

2.2. Correspondence between ordered orthogonal projections and real number triplets

For a fixed curve of the space, the image plane system can be taken in an infinite number of ways. Among the Monge projections that can be added to a fixed curve of the space, there may be those in which the representation of any part of the curve is bijective, and there may be those in which there is a part of the curve whose representation is not bijective.

Theorem 8. *Regarding a spatial object, the same result is obtained during the reconstruction procedure in all Monge projections that can be moved into each other by parallel displacement.*

Proof of Theorem 8. Since the parallel translation is a congruence transformation, the translation does not change the image curves. □

Figure 5 shows some Monge projections that can be transformed into each other by parallel displacement.

Preprints (www.preprints.org) | NOT PEER-REVIEWED | Posted: 3 November 2023 doi:10.20944/preprints202311.0201.v1

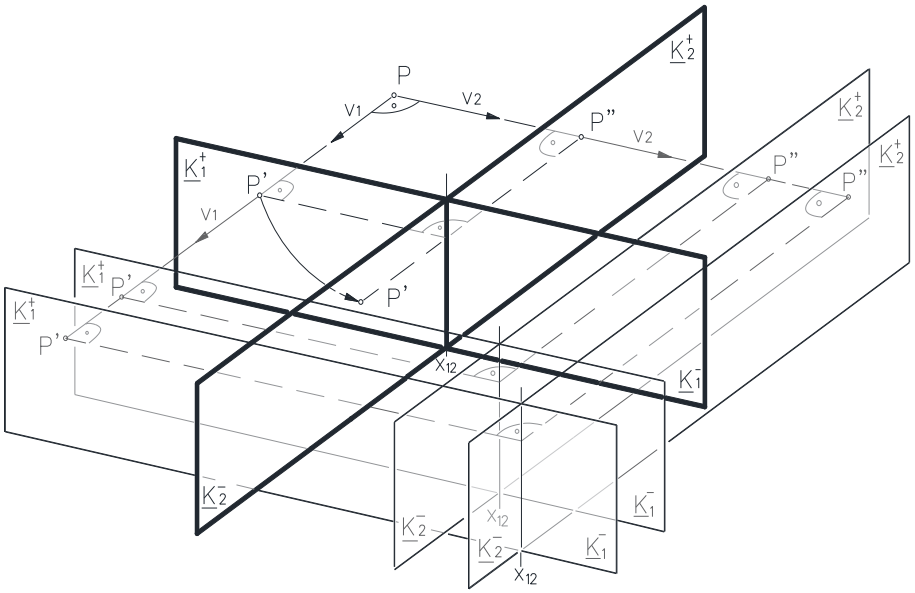

Figure 5. The Monge projections that can be moved into each other with a parallel translation.

Therefore, in what follows, two Monge projections will be considered identical if their reference systems, namely their image plane systems can be moved into each other by parallel displacement. Based on the above, in order to facilitate the further investigations, a point O is fixed in the space, and it is expected that the image planes and projector lines of the Monge projections fit to this point. While the x12 axis, namely the intersection line of the two image planes can be characterized by 2 free parameters, for example two spherical coordinates, the image planes can be described by 1 free parameter in the possibilities of rotation around the x12 axis. Consequently, Monge projections can be described with 3 free parameters in addition to the previous restrictions. After all this, a number triple has been assigned to each Monge projection, whose elements have the geometric meaning of an angle. However, before determining the assignment, it is necessary to define the directed angles of the straight line.

2.2.1. Directed angles of the straight line

In order to create the definitions an O[x, y, z] Cartesian coordinate system has to be fixed in the space.

Definition 2. *The first directed angle α ($0 \le \alpha \le \pi$) of the straight line e passing through the origin point O is the angle, by which the semi-axis x^+ can be rotated towards the first projection e' of the straight line e on the plane [xy] in the direction of the semi-axis y^+, counter- clockwise as viewed from the infinity point of the semi-axis z^+ (Fig. 6). The first directed angle should be interpreted according to $\alpha=0$, if the straight-line e coincides with the axis z. The first directed angle of the straight line bypassing the origin point O is the same as the first directed angle of the straight line parallel to it passing through the origin point O.*

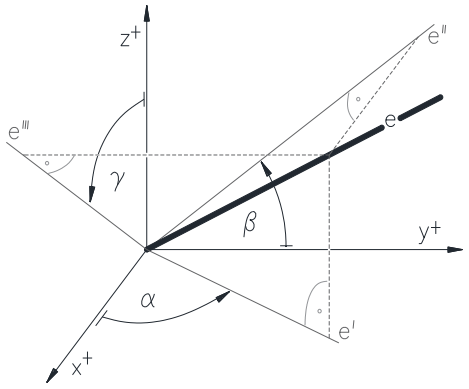

Preprints (www.preprints.org) | NOT PEER-REVIEWED | Posted: 3 November 2023 doi:10.20944/preprints202311.0201.v1

Figure 6. The first directed angle α, the second directed angle β and the third directed angle γ of the straight-line *e*.

Definition 3. *The second directed angle β (0≤β≤π) of the straight line e passing through the origin point O is the angle, by which the semi-axis y^+ can be rotated to the second projection e″ of the straight line e on the plane [yz] in the direction of the semi-axis z^+, counter- clockwise viewed from the infinity point of the semi-axis x^+ (Fig. 6). The second directed angle should be interpreted according to β=0, if the straight-line e coincides with the axis x. The second directed angle of the straight-line e bypassing the origin point O is the same as the second directed angle of the straight line parallel to it passing through the origin point O.*

Definition 4. *The third directed angle γ (0≤γ≤π) of the straight line e passing through the origin point O is the angle by which the semi-axis z^+ can be rotated to the third projection e‴ of the straight line e on the plane [zx] in the direction of the semi-axis x^+, counter-clockwise viewed from the infinity point of the semi-axis y^+ (Fig. 6). The third directed angle should be interpreted according to γ=0, if the straight-line e coincides with the axis y. The third directed angle of the straight-line e bypassing the origin point O is the same as the third directed angle of the straight line parallel to it passing through the origin point O.*

Theorem 9. *If the image planes of the image planes system {$\underline{K}_1$, $\underline{K}_2$} of a Monge projection fit to a fix point O of the space, then the Monge projection is defined by its projector lines v_1 and v_2 passing through the origin O.*

Proof of Theorem 9. The $\underline{K}_1$ image plane will be a plane perpendicular to v_1, $\underline{K}_2$ will be a plane perpendicular to v_2. There are an infinite number of these pairs of planes, but the Monge systems are derived from each other with a parallel display, namely these are equivalent from the point of view of the present examination. □

Theorem 10. *If a given Monge projection is bijective or non-bijective with respect to a given curve g, then the Monge projection obtained by exchanging the image planes $\underline{K}_1$, $\underline{K}_2$ and projector lines v_1, v_2 is also bijective or non-bijective with respect to the given curve g.*

Proof of Theorem 10. By exchanging the image planes $\underline{K}_1$ and $\underline{K}_2$ and the projector lines v_1, v_2 the image curves g′ and g″ of the g curve do not modify, only their comma notations are exchanged, namely g′ becomes g″ and g″ becomes g′. □

The goal is to create a mapping between the Monge projections and the number triplets that clearly characterize them, using the real directed angles defined above, in such a way that all ordered two-images must be discussed.

2.2.2. The relationship between the tripets of directed angles and the Monge projections

Theorem 11. *Besides those Monge projections, whose projector lines v_1 and v_2 fulfil both $v_1 \in [z,x]$ and $v_2 \notin [z,x]$ conditions, define three independent parameters (α,β,γ) in a space fixed Cartesian coordinate system O[x, y, z] as follows: the first directed angle of the first projector line v_1 of the Monge projection should be parameter α, while the second directed angle should be parameter β, and the third directed angle of the second projector line v_2 should be parameter γ.*

Figure 5 shows some Monge projections that can be transformed into each other by parallel displacement.

Remark 1. *The mapping between the Monge projections satisfying the condition given in the Theorem 11 and the directed angles in the range 0≤α, β ,γ≤π is injective, but not surjective.*

Proof of Theorem 11. The proof is divided into two parts. First case when $v_1 \notin$ [zx], second case when $v_1, v_2 \in$ [zx].

1. The first projector line v_1 does not match the coordinate plane [zx] of the O[x, y, z] Cartesian coordinate system. The rotation of x^+ on the plane [xy] with α into the direction of y^+ results the first image v_1' of the projector line v_1, to which the plane $\underline{V}_1$ fits and is perpendicular to the plane [xy]. Then the rotation of y^+ on the plane [yz] with β into the direction of z^+ results the second image v_1'' of the projector line v_1, to which the plane $\underline{V}_2$ fits and is perpendicular to the plane [yz]. Since the assumption $v_1 \notin$ [zx] is hold, there exists an intersection straight line of planes $\underline{V}_1$ and $\underline{V}_2$, and this

Preprints (www.preprints.org) | NOT PEER-REVIEWED | Posted: 3 November 2023 doi:10.20944/preprints202311.0201.v1

intersection straight line is the first projector line v_1 of the sought Monge projection. Then he rotation of z^+ on the plane [zx] with γ into the direction of x^+ results the third image v_2''' of the projector line v_2, to which the plane $\underline{V}_3$ fits and is perpendicular to the plane [zx]. Again, due to our assumption $v_1 \notin$ [zx], the plane $\underline{N}$ perpendicular to v_1 can never coincides with plane $\underline{V}_3$, so there is an intersection straight line of planes $\underline{N}$ and $\underline{V}_3$. This is the second projector line v_2 of the Monge projection (Fig. 7). Based on Theorem 9, the projector lines v_1 and v_2 determine the Monge projection.

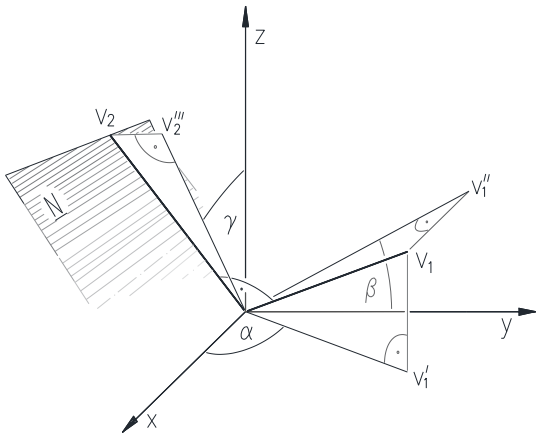

Figure 7. The relationship between the triplet of angle-parameters (α,β,γ) and the projector lines v_1, v_2 of Monge projections in the space fixed Cartesian coordinate system O[x, y, z].

2. The first and second projector lines v_1 and v_2 fit into the coordinate plane [zx] of the O[x, y, z] Cartesian coordinate system. In this case, the corresponding Monge projection is derived from the directed angles triple (α,β,γ) by rotating z^+ in the direction of x^+ by γ in the plane [zx], this will be the second projector line v_2 of the sought Monge projection, and then the first projector line of v_1 is perpendicular to it as shown in Figure 8.

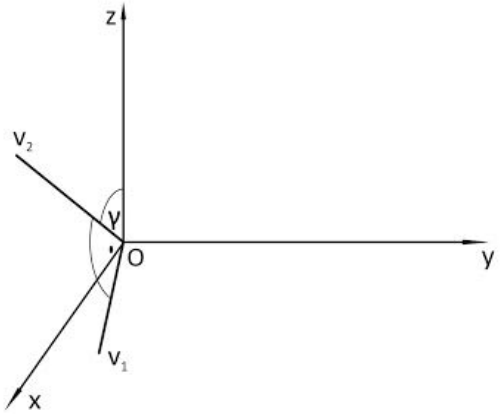

Figure 8. The lines v_1, v_2 of Monge projections fitting to the plane [zx] of the space fixed Cartesian coordinate system O[x, y, z].

It must also be stated here that based on Theorem 9, the projector lines v1, v2 determines the Monge projection. Since v1 has a first and a second, as well as v2 has a third directed angle due to the definition, each Monge projection can be assigned only one number triple. According to the reverse assignment each point of the Monge cuboid defines a triplet of real numbers, the geometric meaning of which is a directed angle, which provides a Monge projection respected to the given curve.

Definition 5. *In the O[α β γ] Cartesian coordinate system, the subset of the elements of the directed angle triples (α, β, γ) within the range [0, π] to which a Monge projection clearly belongs is called a Monge cuboid.*

Preprints (www.preprints.org) | NOT PEER-REVIEWED | Posted: 3 November 2023 doi:10.20944/preprints202311.0201.v1

After examining which of the angle triplets created with angles satisfying the conditions $0 \le \alpha, \beta, \gamma \le \pi$ cannot be assigned a Monge projection, due to the statements made previously, it results that which of the points of the $\pi \times \pi \times \pi$ cube do not belong to the Monge projection to the Monge cuboid.

The points satisfying the following condition are located inside the Monge cuboid as sketched in Figure 9.

$$0 < \alpha < \pi \quad 0 < \beta < \pi/2, \quad \pi/2 < \beta < \pi \quad 0 < \gamma < \pi \tag{1}$$

Points satisfying the following conditions are located on the surface of the Monge cuboid as sketched in Figure 9.

$$\left.\begin{array}{l} -0 < \alpha < \pi, \quad \beta = \pi, \quad 0 < \gamma < \pi \\ -0 < \alpha < \pi, \quad 0 < \beta < \pi/2, \quad \pi/2 < \beta < \pi, \quad \gamma = \pi \\ -\alpha = \pi, \quad \beta = \pi/2, \quad 0 < \gamma < \pi/2, \quad \pi/2 < \gamma < \pi \\ -\alpha = 0, \quad \beta = \pi/2, \quad \gamma = \pi/2 \\ -\alpha = \pi, \quad \beta = 0, \quad \gamma = \pi \end{array}\right\} \tag{2}$$

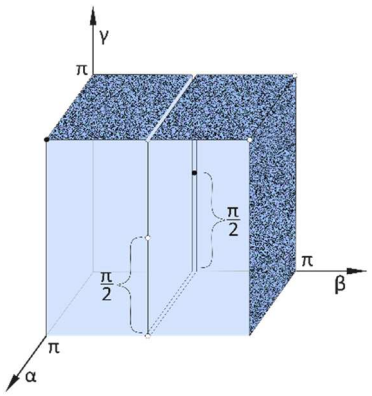

Figure 9. The schematic representation of the inside point and the surface points of the Monge cuboid.

In summary, according to the presented procedure, a Monge projection is assigned to a point of the Monge cuboid by interpreting the triplet of angle parameters as coordinates. In the opposite direction, any point of the Monge cuboid defines a Monge projection by interpreting its coordinates as a triplet of directed angles. A mathematical mapping is created between Monge projections and Monge cuboid points. This method covers all two orthogonal projections assigned to each other that are relevant in engineering. This is suitable for carring out our analyses, because the test of reconstructability with respect to a curve results in the same conclusion by exchanging the first and second views. The presentation of the method was based on what was described in the literature [49].

2.3. Application of the method

During the performance of the method, there are 3 important points to consider:

1. The curve must be positioned in a fixed O[x, y, z] initial Cartesian coordinate system.
2. The direction cone formed from the direction of the tangents of the curve must be determined, that is, the tangents of the curve must be moved parallel to themselves into a properly selected point of the z axis, such as the origin O.
3. Examining the mutual position of the profile planes of the Monge projections and the directional cone, it is necessary to find the cases when they do not have a common line.

The correctness of the method can be immediately checked and verified by the practitioners of descriptive geometry through the examples presented below.

2.3.1. Procedure for the representation of a straight line

It is advisable to choose the mutual position of the straight line and the Cartesian coordinate system as simply as possible. Therefore, it is convenient for the line *e* to lie on a coordinate axis, such as the *z* coordinate axis, as shown in Figure 10.

Preprints (www.preprints.org) | NOT PEER-REVIEWED | Posted: 3 November 2023 doi:10.20944/preprints202311.0201.v1

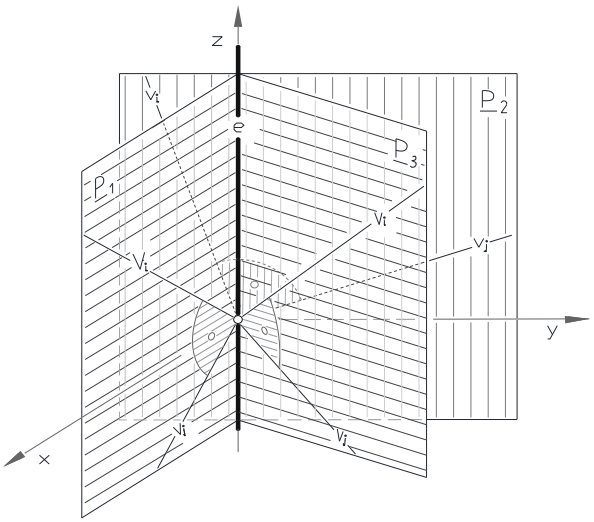

Figure 10. The straight-line *e* fitted to the axis *z* with the profile plane fitted to it in positions $\underline{P}_1$, $\underline{P}_2$ and $\underline{P}_3$, which contains the projector lines $v_{i,j}$ (i,j=1,2 and i≠j), which do not match any of the coordinate axes.

In this case, the direction cone of the straight-line *e* is formed by the tangents moved to the point O characterized by coordinates (0, 0, 0), namely the axis *z* itself. Consequently, in any Monge projection, it is not possible to reconstruct the line *e* from only its two images, in which the profile plane $\underline{P}$ of the Monge projection also fits the axis *z*, namely $\underline{P}$ is an element of the planes series fitting on the axis *z*, unless the straight line *e* is a projector line. In the case of the representation of the line *e* fitting to the coordinate axis *z*, the non-bijective subset of the Monge cuboid can be determined in three position of the profile plane, which are explained in the following:

1. In the first case, the profile plane labeled $\underline{P}_1$ fits on the [zx] coordinate plane, namely $\underline{P}_1 \equiv [zx]$, as well as the projector lines v_1 and v_2 do not fit on either the *z* or *x* coordinate axes. In this case, the subset to be found is declared by angle triples satisfying the following conditions

$$-\alpha = \pi \quad \beta = \pi/2 \quad 0 < \gamma < \pi/2 \quad \pi/2 < \gamma < \pi \tag{3}$$

2. In the second case, the profile plane labeled $\underline{P}_2$ fits on the [yz] coordinate plane, namely $\underline{P}_2 \equiv [yz]$, as well as the projector lines v_1 and v_2 do not fit on either the *y* or *x* coordinate axes. In this case, the subset to be found is declared by angle triples satisfying the following conditions

$$-\alpha = \pi/2 \quad 0 < \beta < \pi/2 \quad \pi/2 < \beta < \pi \quad \gamma = \pi \tag{4}$$

3. In the third case, as outlined in Figure 10, the profile plane in position P3 lies on the z coordinate axis, but does not lie on either of the x or y coordinate axes, and none of the projector lines lie onto the z coordinate axis.

In this case the first directed angle value can be chosen according to the conditions $0<\alpha<\pi/2$ and $\pi/2<\alpha<\pi$. In the case of a fix α value, the second directed angle can be chosen according to the conditions $0<\beta<\pi/2$ and $\pi/2<\beta<\pi$. In the case of a fixed α and β, what conditions γ fulfills was investigated.

To examine the projector lines lying the profile plane P3 the direction vector of the first projector line v1 should be v1(v1x,v1y,v1z), the direction vector of the second projection line v2 should be v2(v2x,v2y,v2z) as shown in 11. Figure.

Preprints (www.preprints.org) | NOT PEER-REVIEWED | Posted: 3 November 2023 doi:10.20944/preprints202311.0201.v1

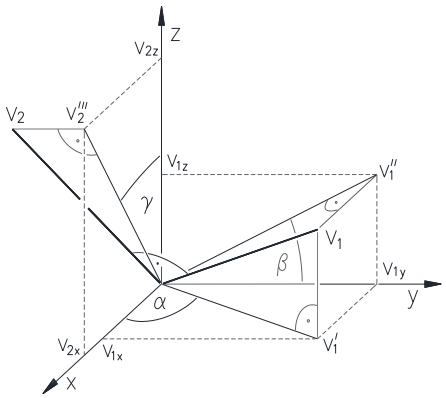

Figure 11. The relationship between the triple of angle parameters (α, β, γ) and the projector lines v_1, v_2 of Monge projections in the space fixed Cartesian coordinate system O[x,y,z].

The **n** normal vector of the first projector plane $\underline{V_1}$ lying to the v_1 and v_2 projector lines should be $\underline{\mathbf{n}}=(v_{1y},-v_{1x},0)$.

Since v2⊥v1 and v2⊥n, due to the following relation

$$\mathbf{v}_2 = \mathbf{v}_1 \times \mathbf{n} \tag{5}$$

the coordinates of the $\mathbf{v}_2$ second projector line are

$$\left(v_{1x} \cdot v_{1z},\ v_{1y} \cdot v_{1z},\ -v_{1x}^2 - v_{1y}^2\right) \tag{6}$$

As it can be seen in Figure 11, in the case of conditions α, β, γ ≠ 0, π, relation

$$\cos^2\alpha = v_{1x}^2 / \left(v_{1x}^2 + v_{1y}^2\right) \tag{7}$$

and based on Figure 11, under the α, β, γ ≠ 0, π conditions, the following simple relationships can be established

$$\left.\begin{aligned} - \quad & tg\alpha = v_{1y}/v_{1x} \\ - \quad & tg\beta = v_{1z}/v_{1y} \\ - \quad & tg\gamma = v_{2x}/v_{2z} \end{aligned}\right\} \tag{8}$$

and the α, β, γ ≠ π/2 exclusions, the following conclusions can be drawn

$$\left.\begin{aligned} - \quad & ctg\alpha = v_{1x}/v_{1y} \\ - \quad & ctg\beta = v_{1y}/v_{1z} \\ - \quad & ctg\gamma = v_{2z}/v_{2y} \end{aligned}\right\} \tag{9}$$

Using the known trigonometric relations presented in (8) and (9), the following equation can be obtained for a fixed pair of (α, β)

$$\gamma = \operatorname{arctg}\left(-\cos\alpha \cdot \sin\alpha \cdot \operatorname{tg}\beta\right) \tag{10}$$

The coordinates of the points belonging to the non-bijective subset of the Monge cuboid fulfill the following conditions in case of the straight line e lying on the z coordinate axis

$$\left.\begin{aligned} & -\ \alpha = \pi \quad \beta = \pi/2 \quad 0 < \gamma < \pi/2 \quad \pi/2 < \gamma < \pi \\ & -\ \alpha = \pi/2 \quad 0 < \beta < \pi/2 \quad \pi/2 < \beta < \pi \quad \gamma = \pi \\ & -\ 0 < \alpha, \beta < \pi/2 \quad \pi/2 < \alpha, \beta < \pi \quad \gamma \neq 0 \Rightarrow \gamma = \operatorname{arctg}\left(-\cos\alpha \cdot \sin\alpha \cdot \operatorname{tg}\beta\right) \end{aligned}\right\} \tag{11}$$

2.3.2. Procedure in the case of the circle representation

Preprints (www.preprints.org) | NOT PEER-REVIEWED | Posted: 3 November 2023 doi:10.20944/preprints202311.0201.v1

The examination has been carried out in the case of a circle with origin center lying on the [xy] plane of the Cartesian coordinate system. In this case, by shifting the tangents of the circle to the origin point O, the special cone of the tangent directions is a series of straight lines in a radial position on the [xy] plane with the O origin as the center. The direction cone of the circle is intersected by the profile plane of every Monge projection passing through the origin, that is, the circle has a tangent in the profile direction. It should be noted that if the profile plane coincides with the plane [xy], the two images of the circle are each a diameter-length section. If the first projector line v_1 or the second projector line v_2 lies in the plane [xy], then one of the images of the circle is a diameter-length section, namely a double projection, so it can be written as a function on the corresponding Cartesian coordinate plane, while the other image is a circle or an ellipse. In this exceptional case, the representation of the circle with the given location is bijective. For the reasons listed earlier, two cases must be considered in the following:

1. If the $v_1 \in [xy]$ and $v_2 \notin [xy]$ are fulfilled, the representation of the given circle is bijective, if the $v_1 \notin x$ as shown in Figure 12a), or $v_1 \in x$ and $v_2 \in z$ as shown in Figure 12b).

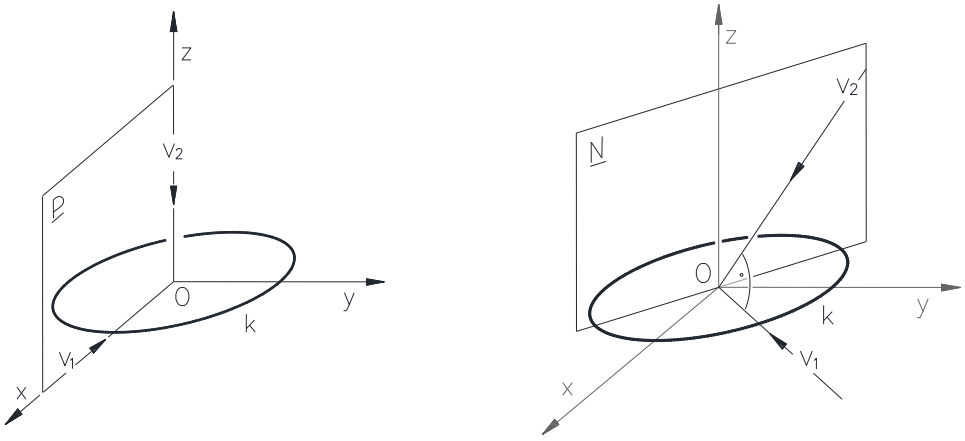

(**a**) (**b**)

Figure 12. The circle fitting on the plane [xy] with O origin center and (**a**) the v_1 projector line lies on the coordinate axis *x*, respectively the v_2 projector line lies on the coordinate axis *z* (**b**) the v_1 projector line lies on the coordinate plane [xy] without coordinate axis and the v_2 projector line on its normal plane N.

2. Among the cases $v2 \in [xy]$ and $v1 \notin [xy]$, the fulfillment of the $v1 \in z$ condition is determined by the directed angles $\alpha=0$, $\beta=\pi/2$ and $\gamma=\pi/2$ as shown in Figure 13. a), so the circle can be clearly represented. If $v2 \in [xy]$ and $v1 \notin [xy]$ are fulfilled as shown in Figure 13.b), the representation of the given circle is bijective.

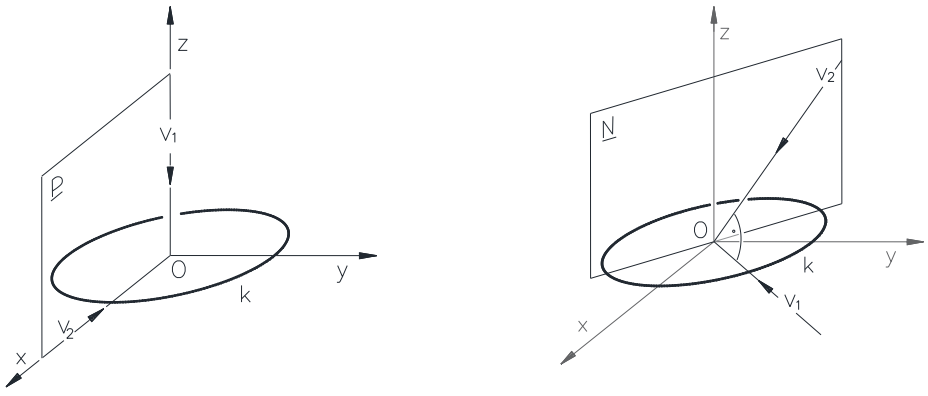

(**a**) (**b**)

Preprints (www.preprints.org) | NOT PEER-REVIEWED | Posted: 3 November 2023 doi:10.20944/preprints202311.0201.v1

Figure 13. The circle fitting on the coordinate plane [xy] with O origin center and (**a**) the v_1 projector line lies on the coordinate axis *z*, respectively the v_2 projector line lies on the coordinate axis *x* (**b**) the v_1 projector line lies on the coordinate plane [xy] without coordinate axes and the v_2 projector line lies on its normal plane N.

Based on the reasoning, the triplet of directed angles that meet the following conditions are interpreted as coordinates and result the points of the bijective part of the Monge cuboid with respect to the circle placed in the determined position

$$\left.\begin{array}{l} -\ 0 < \alpha < \pi \quad \beta = \pi \quad 0 < \gamma < \pi/2 \quad \pi/2 < \gamma < \pi \\ -\ \alpha = \pi \quad \beta = 0 \quad \gamma = \pi \\ -\ 0 < \alpha < \pi \quad 0 < \beta < \pi/2 \quad \pi/2 < \beta < \pi \quad \gamma = \pi/2 \\ -\ \alpha = 0 \quad \beta = \pi/2 \quad \gamma = \pi/2 \end{array}\right\} \tag{12}$$

The three free directed angle parameters satisfying the above conditions result in suitable directions for locating the two CCD cameras, so that the circle can be reconstructed from the two images taken by the cameras.

2.3.3. Presentation of the procedure during the representation of the helix

The center line of the helix should practically lie to the z coordinate axis of the Cartesian coordinate system, as shown in Figure 13.

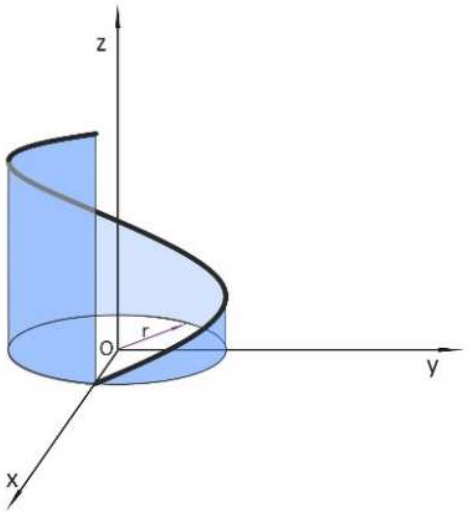

Figure 13. The axis of cylindrical helix fitting to the *z* coordinate axis.

Because of the cyclicity of the curve, the examination of the helix has been performed for one thread pitch. The parametric equation of one thread of the helix with the thread pitch parameter *p* on a cylinder with radius *r* and axis *z* is

$$\left.\begin{array}{l} x = r \cdot \cos\varphi \\ y = r \cdot \sin\varphi \\ z = p \cdot \varphi \end{array}\right\} \tag{13}$$

where $p \in \mathbb{R} \setminus \{0\}$, $r \in \mathbb{R}^+$, $0 \leq \varphi < 2\pi$.
The derivate coordinates of the helix result in the tangent vectors $\mathbf{r}_e$

$$\left.\begin{array}{l} x_e = r \cdot \sin\varphi \\ y_e = -r \cdot cos\varphi \\ z_e = p \end{array}\right\} \tag{14}$$

The direction cone of the helix is created by the tangents moved parallel to themselves to the origin point O. The half opening angle of the direction cone of the tangent vectors is the constant angle ω. In any Monge projection, whose profile plane P2 contains two creator straight lines of the direction

Preprints (www.preprints.org) | NOT PEER-REVIEWED | Posted: 3 November 2023 doi:10.20944/preprints202311.0201.v1

cone of the tangents as shown in Figure 14, the representation of a pitch of the helix results two tangents in profile direction.

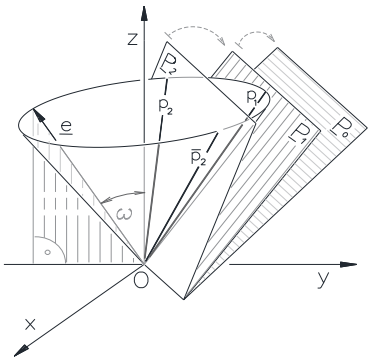

Figure 14. The schematic illustration of the relative positions between the direction cone of the tangents with the z-axis helix and the profile planes of the Monge projections, when they have two common component lines in the $\underline{P_2}$ position, one common component line in the $\underline{P_1}$ position and no common component line in the case of the $\underline{P_0}$ position of the profile plane.

This means that there is a part of the helix whose representation is not clear, namely it is not bijective in the Monge projection belonging to the profile plane at position P2.

If the profile plane of a Monge projection contains one tangent straight line of the cone of tangents to one thread of the helix, as that can be seen in the profile plane at position P1 in Figure 14, then at the point belonging to the profile-oriented tangent straight line of the helix, the tangent straight line intersects the image curves, namely this point is the singular points of the image curves, due to the cyclicity of the helix and its images. In this case, any part of the helix can be clearly reconstructed from its two images. If the cone of the tangential directions of the helix does not have a single common straight line with the profile plane of the Monge projection, namely the profile plane in position P0 as shown in Figure 14. In this case the images of the helix are curtate cycloids (Fig. 15) or planar curves, which are in affine relationship to the curtate cycloids and contain inflection points. In the case of such a Monge projection any segment of the helix can be unambiguously reproducted from its first and second images.

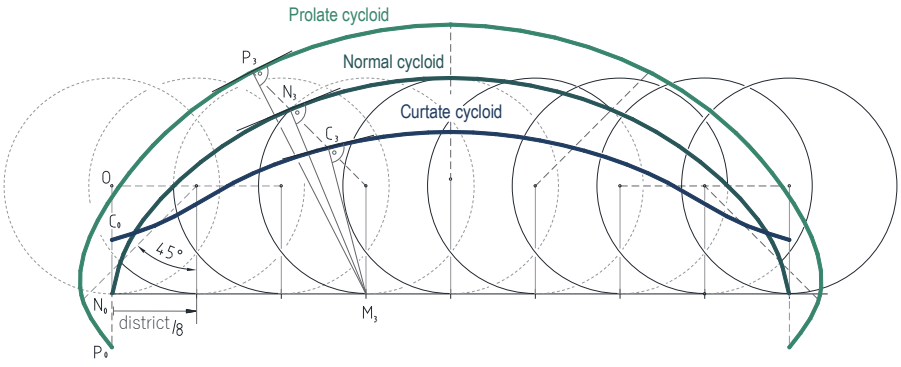

Figure 15. A complete turn of a curtate cycloid created by the inner point C_0 of the circle rolling on a straight line without slipping.

The normal vectors $\mathbf{n}(n_x, n_y, n_z)$ are perpendicular to the tangent planes of the cone of tangent directions of the helix. The normal vectors placed at the origin O create the normal cone, as shown in Figure 16.

All figures and tables should be cited in the main text as Figure 1, Table 1, etc.

Preprints (www.preprints.org) | NOT PEER-REVIEWED | Posted: 3 November 2023 doi:10.20944/preprints202311.0201.v1

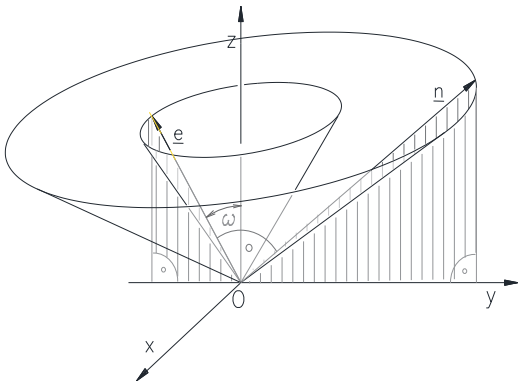

Figure 16. The cone of tangent directions and its normal cone.

That way the generator straight lines of the normal cone of the helix are the normals of the tangent planes of the cone formed by the tangents of the helix. Let the direction vector of the normal cone generator be denoted by **n**. Let the vector **n**(n_x, n_y, n_z) be chosen as the unit vector, namely $|\mathbf{n}|$ and let **z**(0, 0, 1) be the unit vector lying on axis z.

The scalar product of the unit vectors

$$\mathbf{n} \cdot \mathbf{z} = |\mathbf{n}| \cdot |\mathbf{z}| \cdot \cos\left(90° - \omega\right) = \sin\omega \tag{15}$$

and

$$\mathbf{n} \cdot \mathbf{z} = n_x \cdot 0 + n_y \cdot 0 + n_z \cdot 1 \tag{16}$$

so

$$n_z = \sin\omega \tag{17}$$

Due to the condition $|\mathbf{n}| = 1$

$$n_x^2 + n_y^2 + n_z^2 = 1 \tag{18}$$

Substituting result Eq. (17) into Eq. (18) yields a

$$n_x^2 + n_y^2 + \sin^2\omega = 1 \tag{19}$$

and conversion yields the following relation

$$n_x^2 + n_y^2 = \cos^2\omega \tag{20}$$

Eq. (18) is the equation of a circle, in which the $\cos\omega$ is equal to the radius.

It can be established that the tangent direction cone of the stated helix and the profile plane P of a Monge projection, in case

$$n_x^2 + n_y^2 > \cos^2\omega \tag{21}$$

contain two common cone creator straight lines, and in case of

$$n_x^2 + n_y^2 = \cos^2\omega \tag{22}$$

contain one common cone creator straight line, while in case of

$$n_x^2 + n_y^2 < \cos^2\omega \tag{23}$$

no common cone constituent straight line is present.

The aim is to determine the **n**(n_x, n_y, sinω) normals satisfying relations (22) and (23), and the p In summary, the goal is to provide the coordinates α, β, γ of the points of the Monge cuboid that define bijective Monge projections for the given helix.rofile planes perpendicularly to the normals,

Preprints (www.preprints.org) | NOT PEER-REVIEWED | Posted: 3 November 2023 doi:10.20944/preprints202311.0201.v1

than the Monge projections belonging to the profile planes, and finally to specify some conditions of the relations between the α, β, γ coordinates of the points of the Monge cuboid.

In summary, the goal is to provide the coordinates α, β, γ of the points of the Monge cuboid that define bijective Monge projections for the given helix.

Since the projector lines v_1 and v_2 are perpendicular to each other, so their direction vectors $\mathbf{v}_1$ and $\mathbf{v}_2$ are also perpendicular to each other, as a result of which the following relation is fulfilled

$$\mathbf{v}_1 \cdot \mathbf{v}_2 = 0 \tag{24}$$

The relation (24) can be converted into the following forms using the coordinates signed of the direction vectors $\mathbf{v}_1(v_{1x}, v_{1y}, v_{1z})$ and $\mathbf{v}_2(v_{2x}, v_{2y}, v_{2z})$

$$v_{1x} \cdot v_{2x} + v_{1y} \cdot v_{2y} + v_{1z} \cdot v_{2z} = 0 \tag{25}$$

Conversion from relation (25) yields

$$v_{2y} = -\left(v_{1x} \cdot v_{2x} + v_{1z} \cdot v_{2z}\right)/v_{1y} \tag{26}$$

I. In the first part of the examination, the assumptions $\alpha,\beta,\gamma \neq 0, \pi/2, \pi$ are considered.
It is known that

$$\mathbf{n} = \mathbf{v}_1 \times \mathbf{v}_2 \tag{27}$$

which can be written in the following forms

$$n_x = v_{1y} \cdot v_{2z} - v_{2y} \cdot v_{1z} \tag{28}$$

and based on Eq.(8) and Eq.(9)

$$n_x = \left(\operatorname{ctg}\beta + \operatorname{ctg}\alpha \cdot \operatorname{tg}\gamma + \operatorname{tg}\beta\right) \cdot v_{1z} \cdot v_{2z} \tag{29}$$

as well as

$$n_y = v_{1z} \cdot v_{2x} - v_{2z} \cdot v_{1x} \tag{30}$$

and based on Eq.(8) and Eq.(9)

$$n_y = \left(\operatorname{tg}\gamma - \operatorname{ctg}\beta \cdot \operatorname{ctg}\alpha\right) \cdot v_{1z} \cdot v_{2z} \tag{31}$$

furthermore

$$n_z = v_{1x} \cdot v_{2y} - v_{2x} \cdot v_{1y} \tag{32}$$

and based on Eq.(8) and Eq.(9)

$$n_z = \left(-\operatorname{ctg}\alpha - \operatorname{tg}\beta \cdot \operatorname{ctg}\gamma - \operatorname{tg}\alpha\right) \cdot v_{1x} \cdot v_{2x} \tag{33}$$

Since $0 < \omega < \pi/2$, the equality $n_z = \sin\omega \neq 0$ is fulfilled. Using equations (9) and (28)-(33), the following result is obtained

$$n_x/n_z = \left(\operatorname{tg}\alpha \cdot \operatorname{ctg}\gamma + \operatorname{tg}\beta + \operatorname{tg}\alpha \cdot \operatorname{tg}^2\beta \cdot \operatorname{ctg}\gamma\right)/\left(-\operatorname{ctg}\alpha - \operatorname{tg}\beta \cdot \operatorname{ctg}\gamma - \operatorname{tg}\alpha\right) \tag{34}$$

as well as

$$n_y/n_z = \left(\operatorname{tg}\alpha \cdot \operatorname{tg}\beta - \operatorname{ctg}\gamma\right)/\left(-\operatorname{ctg}\alpha - \operatorname{tg}\beta \cdot \operatorname{ctg}\gamma - \operatorname{tg}\alpha\right) \tag{35}$$

Substituting $n_z = \sin\omega$ gives the following results

$$n_x = \sin\omega \cdot \left(\operatorname{tg}\alpha \cdot \operatorname{ctg}\gamma + \operatorname{tg}\beta + \operatorname{tg}\alpha \cdot \operatorname{tg}^2\beta \cdot \operatorname{ctg}\gamma\right)/\left(-\operatorname{ctg}\alpha - \operatorname{tg}\beta \cdot \operatorname{ctg}\gamma - \operatorname{tg}\alpha\right) \tag{36}$$

as well as

$$n_y = \sin\omega \cdot \left(\operatorname{tg}\alpha \cdot \operatorname{tg}\beta - \operatorname{ctg}\gamma\right)/\left(-\operatorname{ctg}\alpha - \operatorname{tg}\beta \cdot \operatorname{ctg}\gamma - \operatorname{tg}\alpha\right) \tag{37}$$

After all this, the following conclusions can be summarized based on the relationships (22)-(23):
If the tangents and axis of a helix form an angle ω, then the triplets (α,β,γ) satisfying the relation

Preprints (www.preprints.org) | NOT PEER-REVIEWED | Posted: 3 November 2023 doi:10.20944/preprints202311.0201.v1

$$((\mathrm{tg}\alpha \text{穋} \mathrm{tg}\gamma + \mathrm{tg}\beta + \mathrm{tg}\,\alpha \cdot \mathrm{tg}^2\,\beta \cdot \mathrm{ctg}\gamma)/(-\mathrm{ctg}\alpha - \mathrm{tg}\beta \text{穋} \mathrm{tg}\gamma - \mathrm{tg}\alpha))^2 + \\ + ((\mathrm{tg}\alpha \cdot \mathrm{tg}\beta - \mathrm{ctg}\gamma)/(-\mathrm{ctg}\alpha - \mathrm{tg}\,\beta \cdot \mathrm{ctg}\,\gamma - \mathrm{tg}\alpha))^2 \leq \mathrm{ctg}^2\,\omega \quad (38)$$

are the cooedinates of the points belonging to the bijective subset of the Monge cuboid.
It can be noted that in the Monge projections defined by number triples satisfying condition (38), the images of the helix contain singular points.

In case of $\omega=\pi/4$ the triplets $\alpha=\pi/6$, $\beta=\pi/6$ and $\gamma=\pi/3$ fulfills the condition (38), so as shown in Figure 17, any section of the helix can be reconstructed from only two of its images.

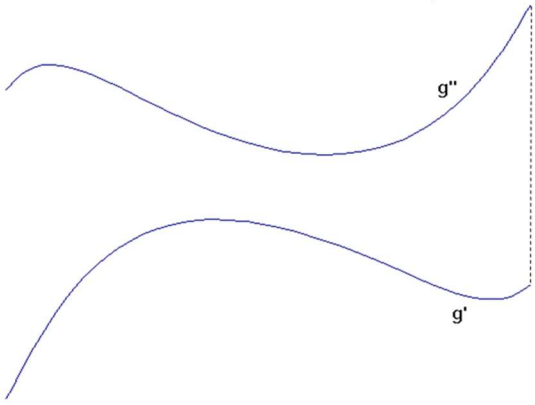

Figure 17. Demonstration of the bijective representation of the helix for the case of $\omega=\pi/4$ in the Monge projection assigned to the triplet of directed angles $(\pi/6,\pi/6,\pi)$ by the computer program developed for this purpose.

Condition (38) is fulfilled for the $\omega=\pi/4$ and for the angular triplet $\alpha=\pi/4$, $\beta=\pi/4$, $\gamma=\pi/4$. Since the left and right sides of condition (38) are equal, the helix has a profile direction tangent intersecting of a complete course of it, so any section of it can be clearly reconstructed from its two images, as shown in Figure 18.

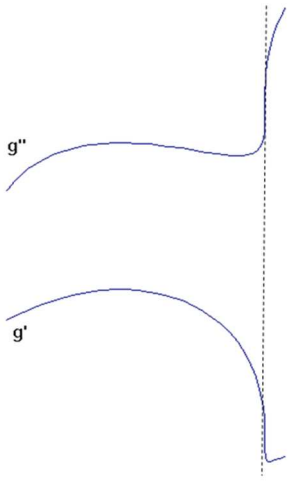

Figure 18. Demonstration of the bijective representation of the helix for the case of $\omega=\pi/4$ in the Monge projection assigned to the triplet of directed angles $(\pi/4,\pi/4,\pi/4)$ by using the computer program created for this procedure.

In the case of $\omega=\pi/4$, the triplet $\alpha=\pi/3$, $\beta=\pi/4$, $\gamma=2\pi/3$ does not fulfill the condition (38), so in the Monge projection belonging to these directed angles, as shown in Figure 19, there are parts of a complete run of the helix that cannot be clearly reconstructed based on their two images alone without additional information.

Preprints (www.preprints.org) | NOT PEER-REVIEWED | Posted: 3 November 2023 doi:10.20944/preprints202311.0201.v1

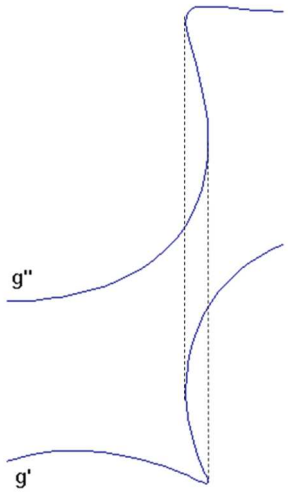

Figure 19. A non-bijective representation of the helix in that Monge projection, which is determined by its projector lines directions calculated from the three directed angles (π/3,π/4,2π/3) with the computer program developed for this purpose, in the case of ω=π/4.

Note that the angles formed by the projection lines and the axis of the helix are greater than ω, then the profile plane of the Monge projection defined by the projection lines intersects the direction cone of the helix in two creator straight lines, so the two image curves g' and g'' have two tangents in the profile direction.

II. In the second part of the examination it must be analyzed how the relation (38) is modified for the coordinates n_x, n_y, n_z of the **n** vectors belonging to the above excluded cases α, β, γ ≠ 0, π/2, π;

1. The examination of the points on the surface of the Monge cuboid must be done in several parts.

1.1. The points determined by the coordinates

- α=π, β=0, γ=π, belong to the non-bijective subset of the Monge cuboid;
- α=0, β=π/2, γ=π/2, belong to the non-bijective subset of the Monge cuboid;

1.2. Among the points defined by coordinates corresponding to the conditions 0<α<π, β=π, 0<γ≤π, those whose coordinates correspond to the following sub-criteria, as the

- 0<α<π, β=π, γ=π/2, always result a bijective Monge projection due to the condition 0<ω<π;
- 0<α<π, β=π, γ=π, always result a non-bijective Monge projections to the given helix, because of the circle shown second image;
- 0<α<π, β=π, 0<γ<π/2, π/2<γ<π, should be assumed in these cases, so that $|\mathbf{v}_1|=1$.

Then the coordinates of direction vector of the first projector line are

$$\mathbf{v}_1(\cos\alpha, \sin\alpha, 0) \tag{39}$$

and the coordinates of directon vector of the second projector line is

$$\mathbf{v}_2(-\sin\alpha, \cos\alpha, \sin\alpha\cdot tg\gamma) \tag{40}$$

The vector product of the $\mathbf{v}_1$ and $\mathbf{v}$ vectors is

$$\mathbf{n} = \left(\sin^2\alpha \cdot tg\gamma\,, -\cos\alpha\cdot\sin\alpha\cdot tg\gamma\,, 1\right) \tag{41}$$

Based on (38), if the condition

$$\sin^4\alpha \cdot tg^2\gamma + \cos^2\alpha\cdot\sin^2\alpha\cdot tg^2\gamma \le ctg^2\omega \tag{42}$$

is fulfilled, the helix representation is bijective in the Monge projections belonging to the studied angle triplets;

Preprints (www.preprints.org) | NOT PEER-REVIEWED | Posted: 3 November 2023 doi:10.20944/preprints202311.0201.v1

1.3. Among the points defined by coordinates corresponding to the conditions $0<\alpha<\pi$, $0<\beta<\pi/2$, $\pi/2<\beta<\pi$, $\gamma=\pi$, those whoose coordinates correspond to the following sub-criteria

- $\alpha=\pi/2$, $0<\beta<\pi/2$, $\pi/2<\beta<\pi$, $\gamma=\pi$ always results non-bijective Monge projections;
- $0<\alpha<\pi/2$, $\pi/2<\alpha<\pi$, $0<\beta<\pi/2$,$\pi/2<\beta<\pi$, $\gamma=\pi$, the $v_{2x}=0$, and n_x, n_z,v_{1x}, $v_{1z} \neq 0$.

Let $n_z = \sin\omega$. Then based on (8), (9), (26), (29), (31), (33) the coordinates of the normal vector are formed as follows

$$n_x = \sin\omega \cdot (-\operatorname{tg}\beta - \operatorname{ctg}\beta)/\operatorname{ctg}\alpha \tag{43}$$

$$n_y = \sin\omega \cdot \operatorname{ctg}\beta \tag{44}$$

$$n_z = \sin\omega \tag{45}$$

When the condition below is met

$$(-\operatorname{tg}\beta - \operatorname{ctg}\beta)^2 / \operatorname{ctg}^2\alpha + \operatorname{ctg}^2\beta \leq \operatorname{ctg}^2\omega \tag{46}$$

in the Monge projections belonging to the sub-conditions defined in this point, the representation of the helix is bijective;

2. Examination of the inner points of the Monge cuboid must also be carried out in several parts.

2.1. Among the points defined by coordinates corresponding to the conditions $\alpha=\pi/2$, $0<\beta<\pi/2$, $\pi/2<\beta<\pi$, $0<\gamma<\pi$, those whoose coordinates correspond to the following sub-criteria

- $\alpha=\pi/2$, $0<\beta<\pi/2$, $\pi/2<\beta<\pi$, $\gamma=\pi/2$, the $v_{1x}=0$, and the $v_2 \in x$, so v_{2y}, $v_{2z}=0$.

Then let $v_{2x}=1$. In addition to the identities $n_x=0$, $n_y= v_{1z}$, $n_z=- v_{1y}= \sin\omega$ the $n_y= -\sin\omega\cdot\operatorname{tg}\beta$ is fulfilled and the

$$\operatorname{tg}^2\beta \leq \operatorname{ctg}^2\omega \tag{47}$$

number triplets satisfying the condition each of them, define a bijective Monge projection for the given helix;

- $\alpha=\pi/2$, $0<\beta<\pi/2$,$\pi/2<\beta<\pi$, $0<\gamma<\pi/2$ $\pi/2<\gamma<\pi$ the $v_{1x}=0$. Since $\gamma\neq\pi/2$, therefore $v_2 \notin [xy]$, so $n_x\neq 0$, and since $\gamma \neq 0$, π and the $v_2 \notin [yz]$, consequently $n_z\neq 0$.

The triplets satisfying the condition

$$((\operatorname{ctg}\beta + \operatorname{tg}\beta) + \operatorname{tg}^2\gamma)^2 / \operatorname{ctg}^2\beta \cdot \operatorname{tg}^2\gamma \leq \operatorname{ctg}^2\omega \tag{48}$$

define each of them a bijective Monge projection for the given helix;

2.2. The points with coordinates corresponding to the conditions $0<\alpha<\pi/2$, $\pi/2<\alpha<\pi$, $0<\beta<\pi/2$, $\pi/2<\beta<\pi$, $\gamma=\pi/2$ define Monge projections who's the second projector line v_2 lies on the [xy] plane, so $v_{2z}=0$. Among the points with such coordinates the triples satisfying the condition

$$\operatorname{tg}^2\beta \cdot (1 + \operatorname{tg}^2\alpha)/(-\operatorname{tg}\beta - \operatorname{tg}\alpha) \leq \operatorname{ctg}^2\omega \tag{49}$$

define each of them a bijective Monge projection for the given helix.

In the case of $\omega=\pi/4$, the number triplet $\alpha=\pi/3$, $\beta=\pi/3$, $\gamma=\pi/2$ does not fulfill the condition, so in the Monge projection corresponding to these number triplets, as shown in Figure 20, the helix has a part which cannot be clearly established from only two image;

Preprints (www.preprints.org) | NOT PEER-REVIEWED | Posted: 3 November 2023 doi:10.20944/preprints202311.0201.v1

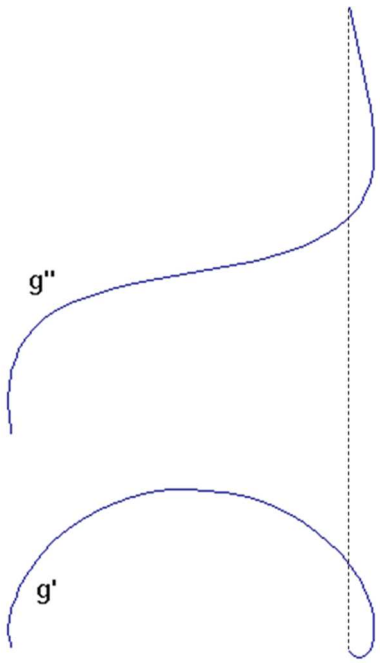

Figure 20. A non-bijective representation of the helix in that Monge projection, which is determined by its projector lines directions calculated from the three directed angles (π/3,π/34,π/2) with the computer program developed for this purpose, in the case of ω=π/4.

If the angle between the axis and tangents of the helix is ω with each other, then the bijective subset of the Monge cuboid for the helix with the specified location is created by number triplets (α, β, γ), that satisfy the following inequalities:

$$
\begin{aligned}
&- \text{ in case } \alpha,\beta,\gamma \neq 0,\ \ \pi/2,\ \ \pi: \\
&\quad ((\mathrm{tg}\alpha \text{穮} \mathrm{tg}\gamma + \mathrm{tg}\,\beta + \mathrm{tg}\,\alpha\cdot \mathrm{tg}^2\,\beta\cdot \mathrm{ctg}\gamma)/(-\mathrm{ctg}\alpha - \mathrm{tg}\beta \text{穮} \mathrm{tg}\gamma - \mathrm{tg}\alpha))^2 + \\
&\quad + ((\mathrm{tg}\alpha\cdot \mathrm{tg}\beta - \mathrm{ctg}\gamma)/(-\mathrm{ctg}\alpha - \mathrm{tg}\,\beta\cdot \mathrm{ctg}\,\gamma - \mathrm{tg}\alpha))^2 \ \leq \mathrm{ctg}^2\,\omega; \\
&- \text{ in case } \ 0<\alpha<\pi,\ \beta=\pi,\ \ \gamma=\pi/2; \\
&- \text{ in case } \ 0<\alpha<\pi,\ \beta=\pi\pi\ 0<\gamma<\pi/2,\ \pi/2<\gamma<\pi: \\
&\quad \sin^4\alpha\cdot \mathrm{tg}^2\,\chi + \cos^2\alpha\cdot \sin^2\alpha\cdot \mathrm{tg}^2\,\gamma \leq \mathrm{ctg}^2\,\omega \\
&- \text{ in case } 0<\alpha<\pi/2,\ \pi\,\pi<\alpha<\pi\pi\,0<\beta<\pi\pi/2\,\pi\,\pi<\beta<\pi\pi\,\gamma=\pi: \\
&\quad (-\mathrm{tg}\beta - \mathrm{ctg}\beta)^2/\mathrm{ctg}^2\alpha + \mathrm{ctg}^2\beta \leq \mathrm{ctg}^2\,\omega \\
&- \text{ in case } \alpha=\pi/2, 0<\beta<\pi\pi/2\,\pi\,\pi<\beta<\pi,\ \gamma=\pi/2: \\
&\quad \mathrm{tg}^2\beta \leq \mathrm{ctg}^2\,\omega \\
&- \text{ in case } \alpha=\pi/2,\ 0<\beta<\pi\pi/,\pi\pi/<\beta<\pi\pi\,0<\gamma<\pi/2,\pi/2<\gamma<\pi: \\
&\quad \left((\mathrm{ctg}\beta+\mathrm{tg}\beta)+\mathrm{tg}^2\gamma\right)^2/\mathrm{ctg}^2\beta\cdot \mathrm{tg}^2\gamma \leq \mathrm{ctg}^2\,\omega \\
&- \text{ in case } 0<\alpha<\pi/2,\ \pi\,\pi/<\alpha<\pi,\ 0<\beta<\pi/2,\ \pi\,\pi<\beta<\pi,\ \gamma=\pi\pi/: \\
&\quad \mathrm{tg}^2\beta\cdot\left(1+\mathrm{tg}^2\alpha\right)/(-\mathrm{tg}\beta - \mathrm{tg}\alpha) \leq \mathrm{ctg}^2\,\omega
\end{aligned}
\tag{50}
$$

The bijective subset of the Monge cuboid for the helix of the specified position in case of the complementary angle ω=π/4, has been displayed by the green inner points and blue bisector and surface points shown in Figure 21.

Preprints (www.preprints.org) | NOT PEER-REVIEWED | Posted: 3 November 2023 doi:10.20944/preprints202311.0201.v1

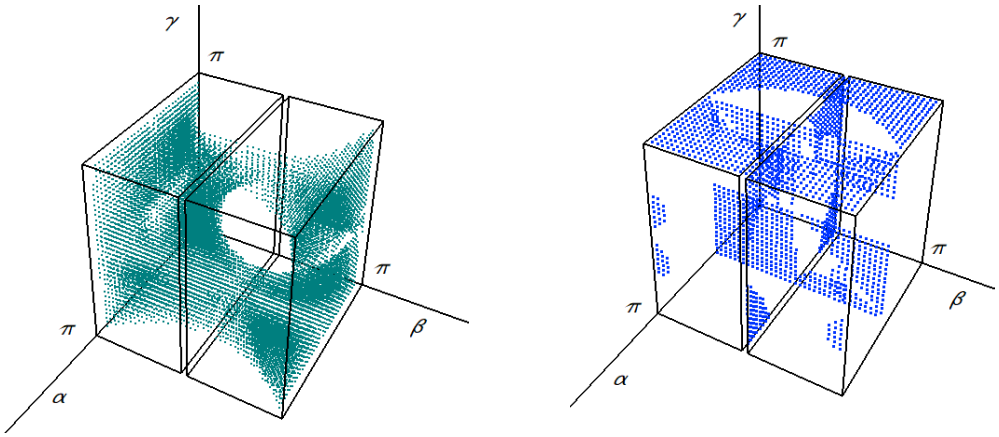

Figure 21. This The inner points of the bijective subset of the Monge cuboid are marked in green (**a**), and its boundary points and bisector points are marked in blue (**b**), relative to the helix with the specified location.

2.3.4. Procedure for a spatial curve representation

Here was also apply our previous statement in this chapter, that if none of the tangents of the curve is in the profile direction, then any part of the curve of the 3D Euclidean space can ceartanly be clearly reconstructed from only two mutually perpendicular orthogonal projections, namely the representation of any part of the curve is bijective. The examination of the spatial curve was carried out in the case of the third-order curve. Let the position vectors $\mathbf{p}_0$ and $\mathbf{p}_3$ pointing to the starting and ending points of the curve P_0 and P_3 be given, as well as the corresponding starting and ending tangent vectors $\mathbf{t}_0$ and $\mathbf{t}_1$, as shown in Figure 22.

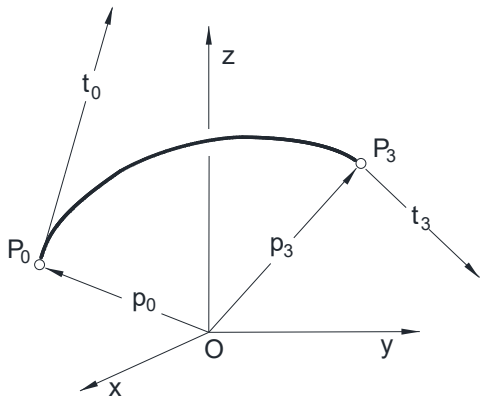

Figure 22. This Schematic illustration of the shape of the Hermite arc of the third-order spatial curve.

The third-order parametrically determined polynomial form of the spatial curve is suitable for the examination of the reconstructibility from its images. The equation of the third-order curve, characterized by the parameter u can be written into the following form

$$\mathbf{r}(u) = \mathbf{a}_3 u^3 + \mathbf{a}_2 u^2 + \mathbf{a}_1 u + \mathbf{a}_0 \tag{51}$$

where practically $u \in [0,1]$, and the derived tangent vectors are given in the form

$$\mathbf{r}_e(u) = \mathbf{e}_1 u^2 + \mathbf{e}_2 u + \mathbf{e}_3 \tag{52}$$

From the condition $u \in [0,1]$ the identities are obtained

Preprints (www.preprints.org) | NOT PEER-REVIEWED | Posted: 3 November 2023 doi:10.20944/preprints202311.0201.v1

$$\left.\begin{aligned}\mathbf{a}_0 &= \mathbf{p}_0\\ \mathbf{a}_1 &= \mathbf{p}_3\\ \mathbf{a}_2 &= -3\cdot\mathbf{p}_0 + 3\cdot\mathbf{p}_3 - 2\cdot\mathbf{t}_0 - \mathbf{t}_3\\ \mathbf{a}_3 &= 2\cdot\mathbf{p}_0 - 2\cdot\mathbf{p}_3 + \mathbf{t}_0 + \mathbf{t}_3\end{aligned}\right\} \quad (53)$$

Based on all this, the tangent vectors can be written in the following form

$$\left.\begin{aligned}\mathbf{e}_1 &= 6\cdot\mathbf{p}_0 - 6\cdot\mathbf{p}_3 + 3\cdot\mathbf{t}_0 + 3\mathbf{t}_3\\ \mathbf{e}_2 &= -6\cdot\mathbf{p}_0 + 6\cdot\mathbf{p}_3 - 4\cdot\mathbf{t}_0 - 2\cdot\mathbf{t}_3\\ \mathbf{e}_3 &= \mathbf{t}_0\end{aligned}\right\} \quad (54)$$

The tangent vectors pass through the origin point O. Any profile plane on which none of the tangent vectors lie determines a Monge projection, which always results in a bijective representation of the given curve. The normal vectors $\mathbf{n}(n_x, n_y, n_z)$ of the planes containing any of the tangent vectors are perpendicular to the tangent vectors lying in it, therefore the following equation is fulfilled, namely

$$\mathbf{n}\cdot\mathbf{r}_e(u) = 0 \quad (55)$$

that can be formed in the following form

$$n_x \cdot r_{ex}(u) + n_y \cdot r_{ey}(u) + n_z \cdot r_{ez}(u) = 0 \quad (56)$$

as well as

$$\left(n_x \cdot e_{1x} + n_y \cdot e_{1y} + n_z \cdot e_{1z}\right)\cdot u^2 + \left(n_x \cdot e_{2x} + n_y \cdot e_{2y} + n_z \cdot e_{2z}\right)\cdot u + \left(n_x \cdot e_{3x} + n_y \cdot e_{3y} + n_z \cdot e_{3z}\right) = 0 \quad (57)$$

To specify the conditions of bijective Monge projections, it is necessary to determine the vectors $\mathbf{n}(n_x, n_y, n_z)$, for which the quadratic equation for the parameter u has no solution. In the following, the vectors $\mathbf{n}(nx, ny, nz)$ in Equation (57) must be determined, for which the quadratic equation with respect to the u parameter has no solution in the case of the specified e_{ij} (i=1,2,3 and j=x,y,z) values. The profile planes determined by such normal vectors do not have a tangent to the examined curve, therefore in the Monge projections related to these profile planes the curve representation is bijective. For the normal vector of the profile plane of all bijective Monge projections, the value of the discriminant of equality (57) is negative, that is

$$(n_x e_{2x} + n_y e_{2y} + n_z e_{2z})^2 - 4(n_x e_{1x} + n_y e_{1y} + n_z e_{1z})(n_x e_{3x} + n_y e_{3y} + n_z e_{3z}) < 0 \quad (58)$$

In order to increase clarity, as published in article [50], writing the constant values of the condition of the negative discriminant in the forms c_i and c_{ij} (i,j=1,2,3) gives the new form of the inequality

$$c_1\cdot n_x^2 + c_2\cdot n_y^2 + c_3\cdot n_z^2 + c_{12}\cdot n_x\cdot n_y + c_{13}\cdot n_x\cdot n_z + c_{23}\cdot n_y\cdot n_z < 0 \quad (59)$$

Monge cuboid points corresponding to the equality conditions formed from the inequality in the following way

$$c_1 n_x^2 + c2 n_x^2 + c_1 n_y^2 + c_3 n_z^2 + c_{12} n_x n_y + c_{13} n_x n_z + c_{23} n_y n_z = 0 \quad (60)$$

separate the points resulting in bijective and non-bijective representations.

Under the conditions $\alpha, \beta, \gamma \neq 0, \pi, \pi/2$ the reference [49], the reconstruction is ensured with the directions of the projector lines determined by the directed angles corresponding to the following condition

$$\begin{aligned}c_1\cdot((\mathrm{tg}\alpha\cdot\mathrm{ctg}\gamma+\mathrm{tg}\beta+\mathrm{ctg}\alpha\cdot\mathrm{tg}^2\beta\cdot\mathrm{tg}\gamma)/(-\mathrm{ctg}\alpha-\mathrm{tg}\beta\cdot\mathrm{ctg}\gamma-\mathrm{tg}\alpha))^2 + c_2\cdot((\mathrm{tg}\alpha\cdot\mathrm{tg}\beta-\mathrm{ctg}\gamma)/(-\mathrm{ctg}\alpha-\mathrm{tg}\beta\cdot\mathrm{ctg}\gamma-\mathrm{tg}\alpha))^2 + c_3\\ + c_{12}\cdot(\mathrm{tg}\alpha\cdot\mathrm{ctg}\gamma+\mathrm{tg}\beta+\mathrm{ctg}\alpha\cdot\mathrm{tg}^2\beta\cdot\mathrm{tg}\gamma)\cdot(\mathrm{tg}\alpha\cdot\mathrm{tg}\beta-\mathrm{ctg}\gamma)/(-\mathrm{ctg}\alpha-\mathrm{tg}\beta\cdot\mathrm{ctg}\gamma-\mathrm{tg}\alpha)^2 +\\ c_{13}\cdot(\mathrm{tg}\alpha\cdot\mathrm{ctg}\gamma+\mathrm{tg}\beta+\mathrm{ctg}\alpha\cdot\mathrm{tg}^2\beta\cdot\mathrm{tg}\gamma)/(-\mathrm{ctg}\alpha-\mathrm{tg}\beta\cdot\mathrm{ctg}\gamma-\mathrm{tg}\alpha) + c_{23}\cdot(\mathrm{tg}\alpha\cdot\mathrm{tg}\beta-\mathrm{ctg}\gamma)/(-\mathrm{ctg}\alpha-\mathrm{tg}\beta\cdot\mathrm{ctg}\gamma-\mathrm{tg}\alpha) < 0\end{aligned} \quad (61)$$

3. Result and application in mechanical engineering practice

Preprints (www.preprints.org) | NOT PEER-REVIEWED | Posted: 3 November 2023 doi:10.20944/preprints202311.0201.v1

One of the special scientific research areas of our Worm School of Science, which deals with the geometry of the tooth surfaces of helicoid surfaces and connected gears [51-56], as well as the machining geometry approach to the mathematical determination in their production, is the analysis of the production geometry development in case of the cylindrical worm with a circular profile in axial section as shown in Figure 23, and the gear connected to it.

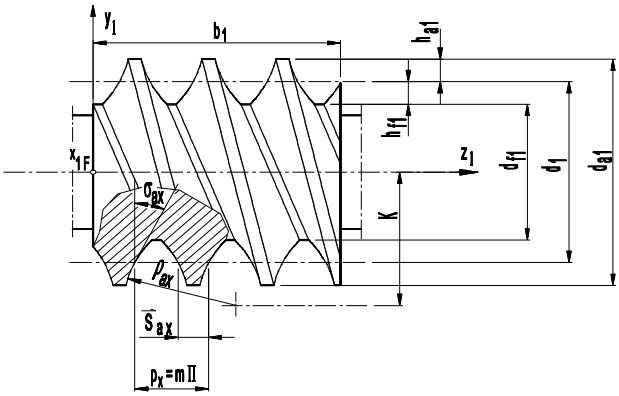

Figure 23. The helicoid worm with arc profile in axial section [40].

The very complicated machining of the gear tooth surface can be done application of the enveloped surface of the worm connected to the gear, by means of the direct motion mapping shown in Figure 24, which can be done with the worm cutter formed from the worm.

Figure 24. The worm gear driving and the worm cutter [56].

In order to increase the precision of the production, the wear of the hob cutting edge can be tested with CCD cameras during production. The theoretical basis of precise analysis with two CCD cameras perpendicular to each other is the Monge mapping. In addition to the ratios of the tool edge size and the distance from the cameras, the geometric corrections to eliminate distortion were performed using the "Contour2" program on the digitized images, which can be considered as the two projection images [52]. The cutting edge is a spatial curve whose digitized images taken with the first and second CCD cameras can be considered as images projected onto the first and second image planes of the Monge mapping. The wear test of the cutting-edge curve with CCD cameras can only be performed if any part of the curve can be clearly reconstructed from its two images.
As shown in Figure 25.a), reconstructibility must be ensured not only for the cutting-edge, but also for the intersected arc between the foot cylinder and the tooth face surface to set the tool into the same position for the testing.

Preprints (www.preprints.org) | NOT PEER-REVIEWED | Posted: 3 November 2023 doi:10.20944/preprints202311.0201.v1

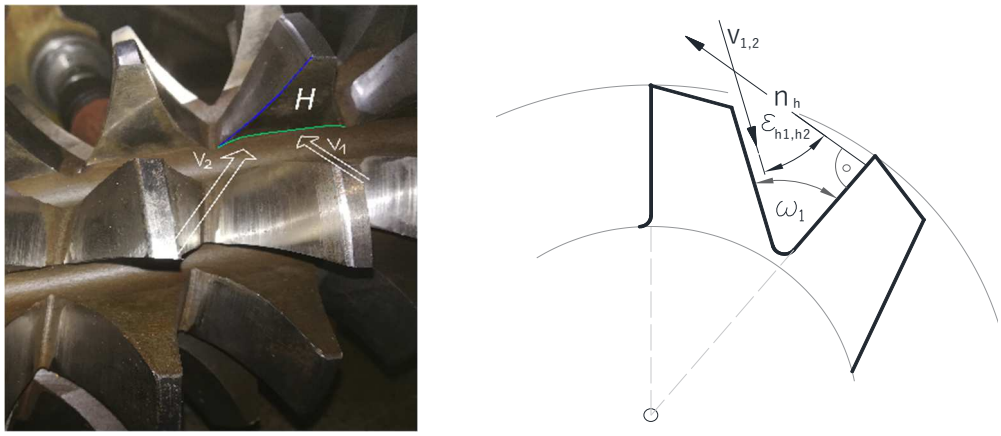

(**a**) (**b**)

Figure 25. The worm gear hob tooth with (**a**) the cutting-edge curve marked with blue line and root cylinder curve marked with green line on the face surface H and the projector directions $\mathbf{v}_1$ and $\mathbf{v}_2$; (**b**) the angle of the chip groove ω_1 in addition to the usual notations [40].

The appropriate form of examination of the cutting-edge curve, which has changed as a result of the operation, is the interpolating third-order Bezier curve, whose connection with the Hermite arc is shown in Figure 26.

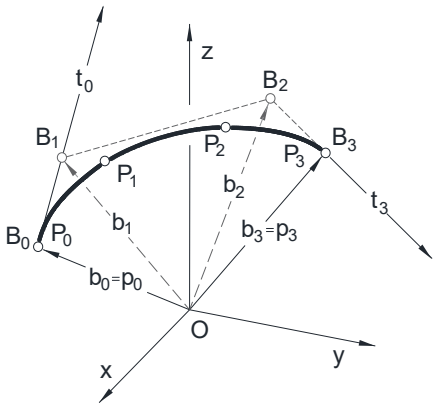

Figure 26. Schematic sketch of the relationship between a Bezier curve and a Hermite arc interpolating to the same spatial curve.

It is advisable to select the cutting-edge points P3 and P0 on the addendum and root cylinder, to appoint the P2 and P1 points between them in proportion to the distance from the axis. The interpolating Bezier curve has four selected points with their position vectors p0, p1, p2, p3 on the cutting edge of the hob, and its parameters u0, u1, u2, u3 satisfy the condition ui ≠ uj, if i ≠ j, as well as u0 = 0 and u3 = 1. The coordinates of position vectors b0, b1, b2, b3 of the control points B0, B1, B2, B3 have to be calculated, which determine the interpolation Bezier curve lying on the selected points thus the following equation is fulfilled

$$\mathbf{b}(u_i) = \mathbf{p}_i \qquad (i = 0,\ldots,3) \tag{62}$$

The well-known form of the Bezier curve using the Bernstein polynomials

$$\mathbf{b}(u) = \sum_{j=0}^{n} B_j^n(u)\mathbf{b}_j \qquad B_j^n(u) = \binom{n}{j} u^j (1-u)^{n-j} \quad (i = 0,\ldots,3) \tag{63}$$

Since the Bezier curve lies at the selected points P_0, P_1, P_2, P_3, it can be given by the following equation

$$\mathbf{b}(u) = \sum_{j=0}^{n} B_j^n(u)\mathbf{b}_j \quad , (j=0,\ldots,3). \tag{64}$$

Preprints (www.preprints.org) | NOT PEER-REVIEWED | Posted: 3 November 2023 doi:10.20944/preprints202311.0201.v1

Appling the $\mathbf{b}(u_i)=\mathbf{p}_i$ (i=0,…,3) equations, the following linear inhomogeneous equation system can be resulted

$$\begin{bmatrix}\mathbf{p}_0\\ \mathbf{p}_1\\ \mathbf{p}_2\\ \mathbf{p}_3\end{bmatrix}=\begin{bmatrix}B_0^3(u_0) & B_1^3(u_0) & B_2^3(u_0) & B_3^3(u_0)\\ B_0^3(u_1) & B_1^3(u_1) & B_2^3(u_1) & B_3^3(u_1)\\ B_0^3(u_2) & B_1^3(u_2) & B_2^3(u_2) & B_3^3(u_2)\\ B_0^3(u_3) & B_1^3(u_3) & B_2^3(u_3) & B_3^3(u_3)\end{bmatrix}\cdot\begin{bmatrix}\mathbf{b}_0\\ \mathbf{b}_1\\ \mathbf{b}_2\\ \mathbf{b}_3\end{bmatrix} \tag{65}$$

The calculation has to be done per coordinate, and its clear solution was the result of the condition specified by us. Thus the bi vectors (i=0,…,3) pointing to control points B0, B1, B2, B3 of the Bezier curve passing through the selected points P0, P1, P2, P3 can be calculated based on Equation (65). The relationship between the p0, p1, p2, p3 position vectors of the control points of the Bezier curve and the position vectors of the start and end points p0 and p3, as well as the start and end tangents t0 and t3 of the Hermite arc can be characterized by the following relations based on the literature [49] and according to the guidance of Figure 26.

$$\left.\begin{aligned}\mathbf{p}_0 &= \mathbf{b}_0\\ \mathbf{p}_3 &= \mathbf{b}_3\\ \mathbf{t}_0 &= 3\cdot\mathbf{b}_1 - 3\cdot\mathbf{b}_0\\ \mathbf{t}_3 &= 3\cdot\mathbf{b}_3 - 3\cdot\mathbf{b}_2\end{aligned}\right\} \tag{66}$$

According to our previous analyses [42] the third-degree Bezier curve approaches the cutting edge within the permitted tolerance zone, if the four points of the cutting edge are selected proportionally between the addendum and dedendum cylinder to specified the interpolating Bezier curve, and these were parameterized in proportional length of chord. The inequality (61) varies according to the coordinates of the points of the cutting edge, according to which the CCD cameras positioned with defined directed angles can in principle produce reconstructable images of the cutting edge.

In the field of view of the CCD cameras placed according to inequality (61), the nearby hob tooth surfaces also require the formulation of additional conditions.

In addition, a third condition is discussed in this article, which eliminates the projector lines, that do not reach in the axis direction the examined cutting edge due to the next hob tooth. If practically the normal vector $\mathbf{n}_h$ of the face surface is determined from the coordinates of the points P_3 and P_0 measured on the cutting edge, as well as the coordinates of the points L_3 and L_0 measured on the root cylinder curve by the cross product of the difference vectors of the position vectors pointing to the points according to the following relation

$$\mathbf{n}_h=(\mathbf{p}_3-\mathbf{p}_0)\times(\mathbf{l}_3-\mathbf{l}_0) \tag{67}$$

then a strong condition has been established. The angles between the $\mathbf{n}_h$ normal vector and the $\mathbf{v}_1$ and $\mathbf{v}_2$ direction vectors of the projector lines can be determined as follows

$$\arccos\frac{\mathbf{n}_h\cdot\mathbf{v}_1}{|\mathbf{n}_h|\cdot|\mathbf{v}_1|}=\varepsilon_{h1} \tag{68}$$

and

$$\arccos\frac{\mathbf{n}_h\cdot\mathbf{v}_2}{|\mathbf{n}_h|\cdot|\mathbf{v}_2|}=\varepsilon_{h2} \tag{69}$$

Furthermore, the angles between the face surface H and the projector lines v1 and v2 projecting into the direction of the axis, can have a maximum value as ω1 as shown in figure 25.b). This means that the minimum value of the angles εh1 and εh2 between the direction vectors of the projector lines and the normal vector nh must be $90^o-\omega_1$ for the chip groove angle of size ω1, as it can be written in the next form

$$\varepsilon_{h1},\varepsilon_{h2}\le 90^\circ-\omega_1 \tag{68}$$

Preprints (www.preprints.org) | NOT PEER-REVIEWED | Posted: 3 November 2023 doi:10.20944/preprints202311.0201.v1

With the visualized procedure, a solution can be selected simultaneously from the subset of solutions in case of three unknown inequalities as shown in Figure 27.

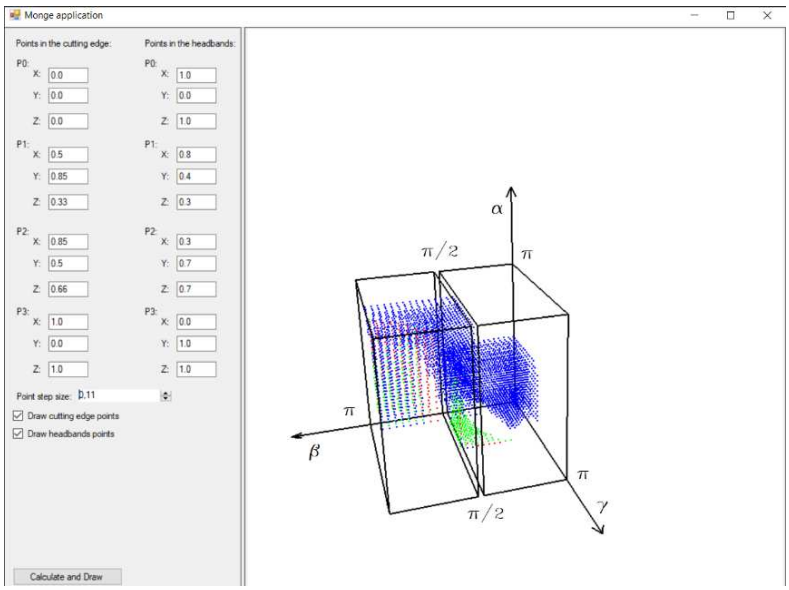

Figure 27. The points of the surfaces bounding the bijective subsets of the Monge cuboid are marked in green for setting the hob, in blue for measuring the wear of the cutting edge, in red for a fixed groove angle.

With this procedure, during the machining process of the parts, it is possible to continuously monitor the size and shape changes that occur during the operation of the cutting edge of the tool, which affects the quality of the machined surface.

4. Discussion

The computer technology evolution made greatly reducing in the cost of designing and prototyping of the mechanizms. The appearing software packages in the market offers and exponentially developing of the computers give to the constractors a huge number of possibilities enabling results to be achieved in a much shorter period of time. The primary task of those engineers who take on tasks from design to implementation is to select compatible softwars that meets industrial requirements. During the design process of the drives, by examining the effect of several possible modifications of geometric parameters of its elements (production accuracy, quality, standard profile angle and gear width) the optimal solution can be selected with a computer program based on the Taguchi method, which method is an optimization procedure based a numerous steps of planning, transacting and interpreting results of matrix tests to determine the most suitable value of the control parameters [57].

A wide selection of tools is available for surface measurement, such as mechanical stylus profilometers, the non-contact optical ones, and the scanning probe microscopes to be chosen in order to take a cross-sectional contour of the air topography data of the investigated surfaces [58]. Several recent reports deal with examinations on optical measurement [59], mainly with diffractive relief structures [60] as well as the interference microscopy [61] furthermore with confocal and spiral scanning [62], factored in comparative papers on various technologies [63]. Some researchers have also discussed the comparability of the surface parameters resulted from the profile and the areal measurements [64,65].

Each of these software's means of communication with the designers and constractors is the Monge's two-view representation of the 3D [66]. *The importance of the production geometry is also shown, for example, by the fact that in order to improve the operating characteristics of hypoid gears, they can be achieved by optimally changing the related tooth surfaces, which can be realized by modifying the settings of the machine tool. The purposes of the multi-objective optimization procedure created with numerical methods were to minimize the maximum contact pressure of the teeth, the transmission error, the average temperature of the gears in their connection field, and to maximize the mechanical efficiency in the case of hypoid gear drives [67]. The wear resistance and service life of cutting tools is also affected by the tribological behavior of the*

 doi:10.20944/preprints202311.0201.v1

different coatings produced with different production parameters [68]. The design and construction of most mechanisms requires a unique approach due to various considerations, which means a constant challenge for today's engineers. A lot of procedures have been prepared to the production geometry generation of machining tools for helicoidal surfaces with constant thread pitch based on the principle of mutual envelopment of surfaces according to the theorems of Olivier and Gohman. A numerical solution suitable for profiling the grinding wheel, that generates the helicoidal surface of the threaded ball-nut motion conversion mechanism is based on the theory of derivation and intersection of surfaces. The points of the approximation tool profile accepted as the final result are the intersection curve points of the derivative surface and the workpiece surface, determined by an initial value problem of an ordinary differential equation system. The smallness of the deviation of the resulted approximation tool profile from the geometrically defined surface, namely its accuracy according to engineering terminology, also depends on the density of the calculated points [69].

The determination of the theoretical tooth surfaces points of the various drives elements must be produced according to the machining process with a mathematical toolbox aimed at the format suitable for the purpose [70]. The theoretical tooth surface can be meshed by its any number of the tooth surface discrete points in the mathematical model made for checking the accuracy. Manufacturing accuracy, referring to the quality of the machined surface, is usually measured with a coordinate measuring machine between the coordinates of the theoretical tooth surface points treated as a reference and the coordinates of the manufactured tooth surface points measured with the coordinate measuring machine. All this can be reviewed in the case of the creation of a mathematical model describing the machining of the tooth surfaces of bevel gears with curved teeth, where the coordinates of the known points of the theoretical tooth surface in the grid points are the reference values on the coordinate measuring machine, which can be compared with the coordinates of the points measured on the manufactured surface [71].

Using exact geometric constructing an interesting motion geometrical result has been published at the operating of the roller freewheel fulfilling the base requirement, that the housing profile, and the hub should create a taper gap, so the roller center has to be fubkcionate along a logarithmic spiral [72].

To achieve the required accuracy of the machining of drives pair elements [73], the tool wear testing is indispensable. Many forward-looking developments have been also made using graphical systems for the further development of technical tools [74]. The simulation and movement study of the Mechanical Integrator 3D Model also can help to understand the processes [75].

During the research into the production geometry of the drive pairs, tests can also be carried out regarding the profile error-free production [76] in order to avoid undercutting. Several geometry-based methods can be used to increase efficiency, such as the coordinate geometry toolbox supplemented with numerical methods [77] and simulation and analytical tools [78] in the case of different type of drives.

By modeling the targeted theoretical tooth sides of the complicated worm gear that fits the cylindrical worm in 3-dimensional CAD software, and by manufacturing the worm gear using a CAM process, and then comparing the contact patterns of the experimental and analytical teeth, it can be concluded that they can be considered to be the same approximation as required in the industry, and as a result, the manufacturing method already validated [79]. The selection of projections is decisive for examining changes in shape and kinematic geometry during machining with high-feed face milling, since at low feed the effect of the material forming of the side edge has been the most critical, the chip becomes deformed perpendicular to it, while the primary part of chip removal gradually moves to an edge perpendicular to the tool axis as the feed increases. For effective chip removal the examination of the two edges separately and together is appropriate using simulations carried out by the AdvantEdge Finite Element Method (FEM) software [80]. The reliability of the finite element and other simulations strongly depends on the applied constitutive models [81]. When forming materials with higher strength in the automotive industry, by increasing fuel efficiency, vehicles also achieve the necessary safety standards, taking into account that during production, the geometry it also varies depending on the properties of the material [82].

An important part of our research work was also the examination of the profile distortions of the grinding wheel during the worm surface machining with a CCD camera [83], which was able to

recognize the contour of the working surface of the grinding wheel, from which it was possible to make a decision about the need for re-sharpening.

5. Conclusions

In the course of our research, during the machining of the worm wheel with a hot plate, we developed a new mathematical procedure for positioning the CCD cameras with mathematical precision to ensure that the cutting-edge curve can be reconstructed from digitized images for wear measurement. The cutting-edge wear tester must be in the same position for each measurement. To set the hob into one position, a surface element had to be selected that does not take part in the machining, therefore its shape does not change. The cutting curve of the root cylinder and the face surface of the hob tooth is suitable for this purpose.

At the same time, by positioning CCD cameras, it is also necessary to ensure the reconstruction of the intersection curve between the face surface of the hob tooth and the bottom cylinder. In order to simultaneously correctly adjust the CCD cameras to the intersected curve between the tooth surface and the root cylinder and to the curve of the cutting edge, so that they only have to be reconstructed from two images taken as perpendicular projections, the data can be derived from the points of the bijective subset of the Monge cuboid with respect to both curves. The directed angles belonging to the point chosen from the bijective subsets of the Monge cuboid determine the directions, in which the CCD cameras should be positioned. This procedure has been developed to measure the wear of the cutting edge of the hob during processing, with which the spatial deformation of the cutting-edge curve can be reconstructed only from digitalized images taken with two CCD cameras using the methods of constructive descriptive geometry. A new third condition has been formulated mathematically, according to which the next tooth of the hob should not be an obstruction to recorde the images taken of the cutting edge, that is, the cameras facing to the direction of the axis could reach the cutting edge. To determine the condition to solve this problem, the relationship between the normal of the face surface of the hob tooth and the projector lines has been determined.

The aim of the aspiration was to make abstract mathematical ideas useful for practical implementations.

Funding: This research received no external funding.

Acknowledgments: I express my gratitude to József Szabó, a retired and then deceased teacher at the University of Debrecen, and to the members of the Science School of the Worm Gear, founded at the University of Miskolc, for their support, who provided me with ideas, encouragement and advice. I express my gratitude to the difiCAD Engineering Office for providing the industrial background necessary for the research.

Conflicts of Interest: The authors declare no conflict of interest.

References

1. Stachel, H. The status of today's Descriptive Geometry related education (CAD/CG/DG) in Europe. In Proceedings of the Annual Meeting of JSGS, 40th anniversary of Japan Society for Graphic Science, 15-20, Tokyo, Japan, 2007. https://doi.org/10.5989/jsgs.41.Supplement1_15
2. Forgó, Z.; Tolvaly-Roșca, F.; Pásztor, J.; Kővári, A. Energy Consumption Evaluation of Active Tillage Machines Using Dynamic Modelling. *Appl. Sci.* **2021**, *11*, 6240. https://doi.org/10.3390/app11146240
3. Suzuki, K. Traditional Descriptive Geometry Education in the 3D-CAD/CG Era. *Journal for Geometry and Graphics* **2014**, *Volume 18*, No. 2, 249–258. https://www.heldermann-verlag.de/jgg/jgg18/j18h2suzu.pdf
4. Tozzi, A.; Mariniello, L. Unusual Mathematical Approaches Untangle Nervous Dynamics. *Biomedicines* **2022**, *10*, 2581. https://doi.org/10.3390/biomedicines10102581
5. Guth, P. L.; Van Niekerk, A.; Grohmann, C. H.; Muller, J. P.; Hawker, L.; Florinsky, I. V.; Gesch, D.; Reuter, H. I.; Herrera-Cruz, V.; Riazanoff, S.; López-Vázquez, C.; Carabajal, C. C.; Albinet, C.; Strobl, P. Digital Elevation Models: Terminology and Definitions. *Remote Sens.* **2021**, *13*, 3581. https://doi.org/10.3390/rs13183581
6. Szarvas, B.; Virág, Z. Seismic effects of rock blasting in the Erdőbénye andesite quarry. *Multidisciplinary sciences* **2021**, *11*, No 1, 159-169. https://doi.org/10.35925/j.multi.2021.1.17
7. Miklós, R.; Lénárt, L.; Darabos, E.; Kovács, A.; Pelczéder, Á.; Szabó, N. P.; Szűcs, P. Karst water resources and their complex utilization in the Bükk Mountains, northeast Hungary: an assessment from a regional hydrogeological perspective. *Hydrogeology Journal* **2020**, *28*, 2159–2172. https://doi.org/10.1007/s10040-020-02168-0
8. Yin, Q.; Chen, Z.; Zheng, X.; Xu, Y.; Liu, T. Sliding Windows Method Based on Terrain Self-Similarity for Higher DEM Resolution in Flood Simulating Modeling. *Remote Sens.* **2021**, *13*, 3604. https://doi.org/10.3390/rs13183604

9. Kundrák, J.; Nagy, A.; Markopoulos, A. P.; Karkalos, N. E. Investigation of surface roughness on face milled parts with round insert in planes parallel to the feed at various cutting speeds. *Cutting & Tools in Technological System* **2019**, *No 91*, ISSN 2078-7405, 87-96. doi.org/10.20998/2078-7405.2019.91.09
10. Cepova, L.; Cep, R.; Chalko, L.; Dvorackova, S.; Trochta, M.; Rucki, M.; Beranek, L.; Mizera, O.; Chyshkala, V. The Effect of Cutting Tool Geometry on Surface Integrity: A Case Study of CBN Tools and the Inner Surface of Bearing Rings. *Applied Sciences* **2023**, *13*, 3543. https://doi.org/10.3390/app13063543
11. Cabezas, S.; Hegedűs, G.; Bencs, P. Transient heat convection analysis of a single rod in air cross-flow. *Pollack Periodica* **2023**, *18*, 23-28. https://doi.org/10.1556/606.2023.00768
12. Cvetković, I. D.; Stojićević, M. D.; Stachel, H.; Milićević, R. G.; Popkonstantinović, B. D. The Man who Invented Descriptive Geometry. *FME Transactions* **2019**, *47*, (2):331-6. doi: 10.5937/fmet1902331C
13. Bucur, C.; Máté, M. Theoretical Peculiarities Regarding the Definition and Representation of the Rolling Surfaces for Chain Transmission. *Procedia Eng.* **2017**, *181*, 206–213. https://doi.org/10.1016/j.proeng.2017.02.372
14. Hervé, J.M. Théodore Olivier (1793–1853). *Distinguished Figures in Mechanism and Machine Science, History of Mechanism and Machine Science* **2007**, 1, 295-318. https://doi.org/10.1007/978-1-4020-6366-4_13
15. Glaeser, G.; Stachel, H. Kinematics—Geometry of Motion. *In: Open Geometry: OpenGL® + Advanced Geometry* **1999**, 451, 229–267. https://doi.org/10.1007/978-1-4612-1428-1_9
16. Attila Körei, A.; Szilágyi, Sz. Displaying Parametric Curves with Virtual and Physical Tools. *The Teaching of Mathematics* **2022**, Vol. XXV, No. 2, 61–73. DOI: 10.57016/TM-EHGC7743
17. Maláková, S.; Urbanský, M.; Fedorko, G.; Molnár, V.; Sivak, S. Design of Geometrical Parameters and Kinematical Characteristics of a Non-circular Gear Transmission for Given Parameters. *Applied Sciences* **2021**, *11*, 1000. https://doi.org/10.3390/app11031000
18. Bendefy A.; Horák P. Gear pair generation with the method of transposed lines of action. In Proceedings of the 14th International Design Conference, DESIGN 2016, Zagreb, Croatia, 16-19, May, 2016, 129-136. https://www.designsociety.org/publication/38822/GEAR+PAIR+GENERATION+WITH+THE+METHOD+OF+TRANSPOSED+LINES+OF+ACTION
19. Bendefy A.; Horák P. Cylindrical Gears with Changing Ratio. *Periodica Polytechnica Mechanical Engineering* **2017**, 61, 130-134. https://doi.org/10.3311/PPme.9870
20. Benotsmane, R.; Dudás, L.; Kovács, G. Newly Elaborated Hybrid Algorithm for Optimization of Robot Arm's Trajectory in Order to Increase Efficiency and Provide Sustainability in Production. *Sustainability* **2021**, *13*, 8193. https://doi.org/10.3390/su13158193
21. Balajti, Z. Development of the Manufacturing Geometry of Conical and Cylindrical Worms by Analyzing of Their Axoids. *Manufacturing Technology* **2020**, *20*, 3-10. DOI: 10.21062/mft.2020.003
22. Güler, E. Generalized Helical Hypersurfaces Having Time-like Axis in Minkowski Spacetime. *Universe*, **2022**, *8*, 469. https://doi.org/10.3390/universe8090469
23. Balajti, Z.; Mándy, Z. Proposed solution to eliminate pitch fluctuation in case of conical screw surface machining by apex adjustment. *Procedia Manufacturing* **2021**, *55*, 266-273. https://doi.org/10.1016/j.promfg.2021.10.038
24. Bonata, C. I.; Bolos, V. The mathematical model of generating kinematic for the worm face gear with modified geometry. *Procedia Technology* **2014**, *12*, 442 – 447. https://doi.org/10.1016/j.protcy.2013.12.512
25. Hogyai, N.; Máté, M.; Tolvaly-Roșca, F.; Drăgoi, M. V. Peculiarities of the Grinding Process of a Gear Hob Helical Rake Face. *Acta Universitatis Sapientiae, Electrical and Mechanical Engineering*, **2021**, *13*, 39-51. DOI: 10.2478/auseme-2021-0004.
26. Tolvaly-Roșca, F.; Forgó, Z.; Máté, M. Evaluation of a Mixed CAD Gear Modeling from Time and Precision Point of View. Procedia Technology 2015, 19, 28-33. https://creativecommons.org/licenses/by-nc-nd/4.0/
27. Ábrahám, Gy.; Wenzelné Gerőfy, K.; Antal, Á.; Kovács, G. *Technical Optics,* 1st ed.; Institute of Mechatronics, Optics, And
Mechanical Engineering Informatics: Budapest University of Technology and Economics, Budapest, Hungary, 2015; p. 308. ISBN 978-963-313-202-9. https://mogi.bme.hu/TAMOP/muszaki_optika/index.html
28. Csoba, I.; Kunkli, R. Rendering algorithms for aberrated human vision simulation. *Visual Computing for Industry, Biomedicine and Art* **2023**, *6*, p. 5. https://doi.org/10.1186/s42492-023-00132-9
29. Prado-Velasco, M.; García-Ruesgas, L. Intersection and Flattening of Surfaces in 3D Models through Computer-Extended Descriptive Geometry (CeDG). *Symmetry* **2023**, *15*, 984. https://doi.org/10.3390/sym15050984
30. Papp, G.; Papp, I.; Kunkli, R. Three-dimensional connection visualization based on tabular data. In Proceedings of the 8th IEEE International Conference on Cognitive Infocommunications (CogInfoCom), pp.: 289-290, Debrecen, Hungary, 11-14 Sept. 2017. https://scholar.google.com/scholar?as_q=Three-dimensional+connection+visualization+based+on+tabular+data&as_occt=title&hl=en&as_sdt=0%2C31
31. Ding, Z.; Liu, S.; Liao, L.; Zhang, L. A digital construction framework integrating building information modeling and reverse engineering technologies for renovation projects. *Automation in Construction* **2019**, *102*, 45–58. DOI: 10.1016/j.autcon.2019.02.012

32. Papp, I.; Zichar, M. 3D Modelling and Printing Interpreted in Terms of Cognitive Infocommunication. *Cognitive Infocommunications, Theory and Applications Topics in Intelligent Engineering and Informatics* **2019**, *13*. https://doi.org/10.1007/978-3-319-95996-2_17
33. Bartonek, D.; Buday, M. Problems of Creation and Usage of 3D Model of Structures and Theirs Possible Solution. *Symmetry* **2020**, *12*, 181. https://doi.org/10.3390/sym12010181
34. Benardos, P.; Vosniakos, G. C. Removed material volume calculations in CNC milling by exploiting CAD functionality. *International Journal of Computer Aided Engineering and Technology* **2018**, *10(5), 495-503.* https://doi.org/10.1504/IJCAET.2018.094343
35. Dudás, I.; Balajti, Z. Modelling and development for describing the bearing pattern of spiroid drives. Proceedings of the Sixth IASTED International Conference on "Robotics and Applications, Cambridge, USA, Oct. 31. – Nov. 02. 2005., 203-208., ISBN 0-88986-521-3. https://www.actapress.com/Abstract.aspx?paperId=22994
36. Bodzás, S.; Békési, Z.; Kertész, J.; Szorcsik, T. The CAD Modelling Possibilities of Gear Pairs by Two Ways in the Mechanical Engineering Practice. *International Journal of Engineering and Management Sciences* **2021**, *6(2)*, 205–219. DOI: 10.21791/IJEMS.2021.2.17.
37. Kundrák, J.; Felhő, C.; Nagy, A. Analysis and Prediction of Roughness of Face Milled Surfaces using CAD Model. *Manufacturing Technology* **2022**, *22* (5), 558-572. DOI: 10.21062/mft.2022.061
38. Máté, M.; Tolvaly-Roșca, F.; Hodgyai, N.; Drăgoi, M.V. A new approach of defining the grinding wheel profile of the Gear Hob's Rake Face. In Proceedings of the IEEE Joint 22nd International Symposium on Computational Intelligence and Informatics and 8th International Conference on Recent Achievements in Mechatronics, Automation, Computer Science and Robotics (CINTI-MACRo 2022), Budapest, Hungary, 21-22, November, 2022. DOI: 10.1109/CINTI-MACRo57952.2022.10029498.
39. Hogyai, N.; Drăgoi, M. V.; Tolvaly-Roșca, F.; Máté, M. About the Grinding of Gear Hob's Rake Face. *Papers on Technical Science – International Scientific Series of the Transylvanian Museum Society*, **2022**, *16*, 31-35. https://doi.org/10.33894/mtk-2022.16.06
40. Dudás, I. *The Theory and Practice of Worm Gear Drives*; Penton Press: London, UK, 2000.
41. Olivier, Th. Theorie geometrique engrenager, Maurice Daumas, Paris, 1842. https://archive.org/details/thoriegomtrique01olivgoog
42. Balajti, Z. Development of Production Geometry of Kinematical Drive Pairs. PhD Dissertation, University of Miskolc, Miskolc, Hungary, 2007, p. 171. (In Hungarian) http://midra.uni-miskolc.hu/document/5519
43. Bodzás, S.: Manufacturing of spur gears having normal teeth on different pressure angles by module disc milling cutter. *International Review of Applied Sciences and Engineering* **2022**, *13*, 3, 321–334. DOI:10.1556/1848.2022.00418
44. Tomori, Z. An Optimal Choice of Profile Shift Coefficients for Spur Gears. *Machines* **2021**, *9*, 106. https://doi.org/10.3390/ machines9060106.
45. Meng, Q.; Zhao, Y.; Yang, Z. Curvature interference characteristic of conical worm gear. *Forsch Ingenieurwes* **2019**, *83*, 759–773. https://doi.org/10.1007/s10010-019-00372-3
46. Pavlenko, S.; Mascenik, J.; Krenicky, T. Mathematical Modeling of Drive and Dynamic Load of Teeth of Cylindrical Worm Gear. 2022, In *Sustainable Management of Manufacturing Systems in Industry 4.0*, 1st ed.; Editor 1, A., Editor 2, B., Eds.; Publisher: Publisher Location, Country, 2007; Volume 3, pp. 61-84. DOI:10.1007/978-3-030-90462-3_5
47. Balajti, Z. Examination and adjustment of bearing pattern in case of helicoid drives. *Procedia CIRP* **2018**, *77*, 267–270, ISSN 2212-8271. https://www.sciencedirect.com/journal/procedia-cirp/vol/77/suppl/C
48. Hungarian Scientific Research Fund-OTKA No T026566 Theme manager Prof. Dr. Dr. h. c. Dudás, I. DSc. Development of CCD cameras systems to the area of machine industry. Miskolc; 2002.
49. Balajti Z. Theoretical analysis and application of the Monge representation in engineering practice. Publisher: Gazdász Elasztik Ltd. University of Miskolc, Hungary, 2015, ISBN: 978-963-358-097-4, 101 p. https://www.researchgate.net/publication/372855431_A_Monge_abrazolas_elmeleti_elemzese_es_alkalmazasa_a_mernoki_gyakorlatban_Miskolc_2015_ISBN_978-963-358-097-4_101_o
50. Balajti, Z.; Dudás, I. The Monge Theorem and Its Application in Engineering Practice. *International Journal of Advance in Manufturing Technolology*, **2017**, *91*, 739–749. https://doi.org/10.1007/s00170-016-9763-1.
51. Dudás, I.; Bányai, K. ; Bodzás, S. Finishing production of spiroid worm shaft by varied centre distance and by appling grinding wheel banking angle correction. *International Review of Applied Sciences and Engineering* **2016**, *(7)* 13-19. https://akjournals.com/view/journals/1848/7/1/article-p13.xml
52. Dudás, L. Modelling and simulation of a new worm gear drive having point-like contact. *Eng. Comput.* **2013**, *29*, 251–272.
53. Bodzás, S. Connection analysis of surfaces of conical worm, face gear and tool. PhD Dissertation, University of Miskolc, Miskolc, Hungary, 2016, p. 120. (In Hungarian) http://midra.uni-miskolc.hu/document/18016/11619.pdf
54. Mándy, Z. Intelligent manufacturing system and geometrically exact manufacture of the helicoid surfaces. PhD Dissertation, University of Miskolc, Miskolc, Hungary, 2022, p.105. (In Hungarian) Academic leader:

Z. Balajti. Qualification: Summa cum laude. http://193.6.1.94:9080/JaDoX_Portlets/documents/document_40897_section_38553.pdf
55. Ábel, J. Computer based constructive geometric and analytical development of the manufacturing geometry of worm gear drive pairs. PhD Dissertation, University of Miskolc, Miskolc, Hungary, 2023, p. 99. (In Hungarian) Academic leader: Z. Balajti. Qualification: Summa cum laude. http://midra.uni-miskolc.hu/document/43049/41118.pdf
56. Balajti, Z. Determination of Undercutting Avoidance for Designing the Production Technology of Worm Gear Drives with a Curved Profile. *Machines* **2023**, *11*, 56. https://doi.org/10.3390/machines11010056
57. Stanojevic, M.; Stojanovic, B.; Bankovic, N. Analysis of Influential Geometric Parameters on the Safety Factor on the Sides of Gear Pairs in the Gearbox Using Taguchi Method. In Proceedings of the 11th international conference on Quality System Condition for Successful Business and Competitiveness, Kopaonik, Serbia, 17-19 May 2023. https://www.researchgate.net/publication/373160923_ANALYSIS_OF_INFLUENTIAL_GEOMETRIC_PARAMETERS_ON_THE_SAFETY_FATOR_ON_THE_
58. SIDES_OF_GEAR_PAIRS_IN_THE_GEARBOX_USING_TAGUCHI_METHOD
59. Gao, W.; Haitjema, H.; Fang, F.Z.; Leach, R.K.; Cheung, C.F.; Savio, E.; Linares, J.M. On-machine and in-process surface metrology for precision manufacturing. *CIRP Ann.* **2019**, *68*, 843–866.
60. Jiao, F.; Liu, L.; Cheng, W.; Li, C.; Zhang, X. Review of optical measurement techniques for measuring three-dimensional topography of inner-wall-shaped parts. *Measurement* **2022**, *202*, 111794.
61. Lu, W.; Chen, S.; Zhang, K.; Zhai, D. Characterization of diffractive relief structures over large areas by stitching interference microscopic topography. *Measurement* **2022**, *202*, 111850.
62. Guo, J.; Zhai, D.; Lu, W.; Chen, S. Topography measurement of helical grooves on a hemisphere based on stitching interference microscopy. *Opt. Laser Technol.* **2022**, *152*, 108133.
63. Ying, R.; Cui, Y.; Huang, J.; Liang, D.; Wang, Y. Precise measurement of surface topography with microstructures based on differential confocal and spiral scanning. *Measurement* **2021**, *184*, 110004.
64. Leksycki, K.; Królczyk, J.B. Comparative assessment of the surface topography for different optical profilometry techniques after dry turning of Ti6Al4V titanium alloy. *Measurement* **2021**, *169*, 108378.
65. Schmidt, J.; Thorenz, B.; Schreiner, F.; Döpper, F. Comparison of areal and profile surface measurement methods for evaluating surface properties of machined components. *Procedia CIRP* **2021**, *102*, 459–464.
66. Svetlik, J.; Baron, P.; Dobransky, J.; Kocisko, M. Implementation of computer system for support of technological preparation of production for technologies of surface processing. In *Applied Mechanics and Materials, Proceedings of the ROBTEP 2014: 13th International Conference on Industrial, Service and Humanoid Robotics, High Tatras, Slovakia, 15–17 May 2014*; Trans Tech Publications Ltd.: Zurich, Switzerland, 2014; Volume 613, pp. 418–425. ISBN 978-303835202-0.
67. Stamenović, B.; Stoimenov, M.; Popkonstantinovic, B.; Jeli, Z. Presses for Designing Flexible Pipes Correction, Finite Elements Analysis and Prepearing "G" Code for Construction Elements of Plasma Cutter. In Proceedings of the 4th International Scientific Conference on Geometry and Graphics moNGeometrija, Vlasina, Serbia, 20-22, June, 2014, 141-156. http://mongeometrija.com/konferencije/mongeometrija-2014
68. Simon, V. Multiobjective optimization of hypoid gears to improve operating characteristics. *Mechanism and Machine Theory*, **2019**, *146*, 905-914. https://doi.org/10.1007/978-3-030-20131-9_90
69. Jakab, M.; Ali, O.I.; Gyurika, I.G.; Korim, T.; Telegdi, J. The Tribological Behavior of TiN/TiC CVD Coatings under Dry Sliding Conditions against Zirconia and Steel Counterparts. *Coatings* **2023**, *13*, 832. https://doi.org/10.3390/coatings13050832
70. Hegedűs, G. Manufacturing Parameters Determination on Ball Nut Grinding. *Design of Machines and Structures*, **2015**, 5, 1, 33-38. HU ISSN 2064-7522 online, https://www.uni-miskolc.hu/dms/docs/dms_vol5_nr1_2015.pdf
71. Dóka T.; Horák P. An Approach to Creating a Simple Digital Twin for Optimizing a Small Electric Concept Vehicle Drivetrain. In Proceedings of the 34th International ECMS Conference on Modelling and Simulation, European Council for Modelling and Simulation (ECMS), 9-12, June, 2020, 328-333. http://doi.org/10.7148/2020
72. Várkuli, M.; Bognár, G.; Szente, J. Determination of Tooth Surface Points on Bevel Gears for Checking on a Coordinate Measuring Machine. *Design of Machines and Structures*, **2023**, *13*, 1, 131–139. https://doi.org/10.32972/dms.2023.011
73. Bihari, Z.; Szente, J. Determination of ideal curve having constant wedge angle for roller freewheels. *Design of Machines and Structures*, **2012,** 2, 1, 15-24. https://www.uni-miskolc.hu/dms/docs/dms_vol2_nr1_2012_contents.pdf
74. Bercsey, T.; Horák, P. Calculation of the Efficiency of ZTA-Type Worm Gear Drives on the Base of The Ethd Lubrication Theory in Proceedings of the 5th International Meeting of the Carpathian Region Specialists in the Field of Gears, Bai Mare, Romania, 21, May, 2004, 34-38. https://www.researchgate.net/publication/237236853_5th_INTERNATIONAL_MEETING_OF_THE_CARPATHIAN_REGION_SPECIALISTS_IN_THE_FIELD_OF_GEARS_CALCULATION_OF_THE_EFFICIEN

CY_OF_ZTA-TYPE_WORM_GEAR_DRIVES_ON_THE_BASE_OF_THE_ETHD_LUBRICATION_THEORY

75. Jeli, Z.; Komatin, M.; Popkonstantinovic, B.; Regodic, M. *Usage of modern graphical presentations in development of technical systems*. In Proceedings of the 3th International Conference moNGeometrija, Novi Sad, Serbia, 21-24, June, 2012, pp. 553-564. ISBN 978-86-7892-405-7, http://mongeometrija.com/media/mongeometrija/2012/MoNGeometrija_2012_Zbornik.pdf
76. Popkonstantinovic, B.; Stojicevic, M.; Jeli, Z.; Obradovic, M.; Dragos-Laurentiu, P.: Simulation and Motion Study of Mechanical Integrator 3D Model. *FME Transactions*, **2019**, *47*, 2, 299-303. https://www.mas.bg.ac.rs/_media/istrazivanje/fme/vol47/2/12_b_popkonstantinovic_et_al.pdf
77. Máté, M.; Hollanda, D.; Tolvaly-Roşca, F.; Forgó, Z.; Egyed-Faluvégi, E. Synthesis of a Profile Errorless Involute Shaper Cutter with Cylindrical Rake Face. In Proceedings of the 2019 IEEE 19th International Symposium on Computational Intelligence and Informatics and 7th IEEE International Conference on Recent Achievements in Mechatronics, Automation, Computer Sciences and Robotics (CINTI-MACRo), Szeged, Hungary, 14-16 November 2019; pp. 71–78. https://doi.org/10.1109/CINTI-MACRo49179.2019.9105302.
78. Máté, M.; Hollanda, D. *Numerical Evaluation of the Shaper Cutter with Cylindrical Rake Face. Papers on Technical Science*, **2020**, *12*. 55-62. ISSN 2601-5773, https://doi.org/10.33894/mtk-2020.12.08
79. Hodgyai, N.; Tolvaly-Roșca, F.; Máté, M. The Conditions of Undercut by Shaping Using a Rounded Profile Gear Shaper Cutter. *Pap. Tech. Sci. Tech. Sci. Dep. Transylv. Mus.-Soc.* **2021**, *14*, 30–36. (In Romania)
80. Kawasaki, K.; Tsuji, I. Manufacturing Method for Large Cylindrical Worm Gear Set of ISO Type I on Universal CNC Machine Tools. *J. Manuf. Mater. Process.* **2023**, *7*, 53. https://doi.org/10.3390/jmmp7020053
81. Karpuschewski, B.; Kundrák, J.; Felhő, C.; Varga, G.; Sztankovics, I.; Makkai, T.; Borysenko, D. Preliminary Investigation for the Effect of Cutting Tool Edge Geometry in High-Feed Face Milling. In Proceedings of the Vehicle and Automotive Engineering 2: Lecture Notes in Mechanical Engineering, 241-245, Miskolc, Hungary, 9, May, 2018. https://link.springer.com/chapter/10.1007/978-3-319-75677-6_20
82. Kuznetsov, V.; Smolin, I.; Skorobogatov, A.; Akhmetov, A. Finite Element Simulation and Experimental Investigation of Nanostructuring Burnishing AISI 52100 Steel Using an Inclined Flat Cylindrical Tool. *Appl. Sci.* **2023**, *13*, 5324. https://doi.org/10.3390/app13095324
83. Gál, V.; Lukács, Z. Effect of Cooling Channels to the Press Hardening Tools Temperature. In Proceedings of the Vehicle and Automotive Engineering 3: Lecture Notes in Mechanical Engineering, 312-320, Miskolc, Hungary, 25, November, 2020. https://doi.org/10.1007/978-981-15-9529-5_28
84. Varga, G.; Balajti, Z.; Dudás, I. Advantages of CCD Camera Measurements for Profile and Wear of Cutting Tools. *Journal of Physics Institute of Physics Publishing in London*, **2005**, *Conference Series 13*, 159-162. doi: 10.1088/1472-6596/13/1/037